The Acoustics of a Tenor Recorder

by

D. D. McKinnon

A thesis submitted to the

Faculty of the College of Arts & Sciences of the

University of Colorado in partial fulfillment

of the requirements for the degree of

Bachelor of Arts

Department of Physics

2009

This thesis entitled:
The Acoustics of a Tenor Recorder
written by D. D. McKinnon
has been approved for the Department of Physics

_____

Prof. John Price

_____

Prof. John Cumalat

_____

Prof. Peter Kratzke

Date _____

McKinnon, D. D. (B.A., Physics)

The Acoustics of a Tenor Recorder

Thesis directed by Prof. John Price

The study of acoustics is rooted in the origins of physics, yet the dynamics of flue-type instruments are still only qualitatively understood. Our group has developed a measurement system, the Acoustic VNA, which can precisely determine acoustic wave amplitudes of the lowest mode propagating in a cylindrical waveguide. I used the AVNA to study a musical oscillator, the tenor recorder. The recorder consists of two components, an air-jet amplifier driven by the player's breath and a cylindrical waveguide resonator with an effective length that may by varied by covering or uncovering finger holes. Previous research on the recorder has focused on understanding the resonator frequencies in some detail, but has only provided a rough understanding of the air-jet. In particular, there is not yet a quantitative understanding of how the pitch varies with blowing pressure for a given fingering. I designed several experiments to provide a quantitative picture of how the air-jet behaves at different blowing pressures and discovered that higher blowing pressures lead to stronger amplification at higher frequencies. Later, using a dimensionless quantity known as the Strouhal number, I showed that maximum amplification always occurs when the oscillating air-jet is allowed approximately one wavelength between the duct exit and the labium. This physical situation is corroborated by Schlieren imagery done by M.P. Verge and my approximate efficiency calculations based on the power spectra.

Dedication

To my parents for their unconditional love and support.

Contents

Tables

Table

Figures

Figure

Chapter 1

Why Study Acoustics?

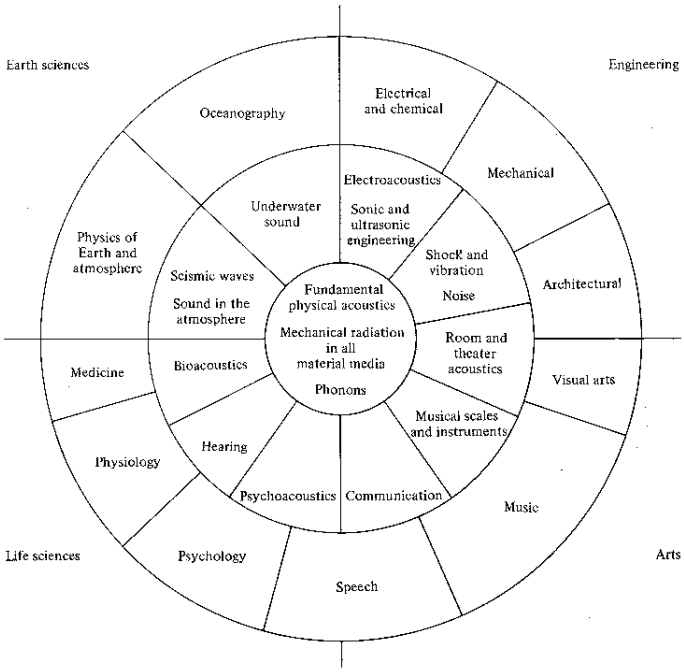

Figure 1.1: Current acoustics research spans a wide gamut of fields and has applications in many areas [1].

Occasionally the question of why study the recorder at all arises. Physicists may wonder how studying a musical instrument, much less one that has been essentially relegated to obscure baroque ensembles and elementary school classrooms, could help advance science. The fact remains, however, that acoustics research draws inspiration from a diverse set of real-world problems and has applications in a wide range of

fields. Fundamental work in acoustics is related to the existence of phonons, quantitized vibrational modes relating to solid state physics [2]. More applied fields range from biologists studying the physiology of hearing and comprehension to geophysicists studying pressure wave propagation through the earth to engineers helping architects to design buildings with certain acoustic qualities.

My research on the recorder is two-fold in importance. First, no one has a solid, quantitative understanding of how flue instruments actually work. If an engineer were to go work for Yamaha in the motorsports division, and he were assigned to design a new internal combustion engine to power a new motorcycle, he could easily do so from scratch. Thousands of papers have been published on every facet of motor design. Everything from the cylinder wall thickness to the cam timing has been extensively studied and the engineer could, in theory, design a novel engine from scratch simply based on previous research. If the same engineer, however, were to go work for Yamaha's musical instrument division, he could not possibly hope to design even a simple recorder from scratch. Very little research exists to demonstrate how changing different aspects of the air-jet geometry, such as the $fracWh$ ratio or labium position, affects the sound radiated. Rather, flue-type instruments have been around for several thousand years and have slowly evolved into their present form. The engineer unlucky enough to be assigned to design a novel new flue instrument would have only tradition and a small dash of science to aid him in his quest. Second, understanding the unstable air-jet has potential ramifications for fluid dynamicists. Rayleigh and Helmholtz were deeply concerned by the mechanics of an oscillating air-jet and, aside from simple models that ignore viscosity and other real world factors like vortex shedding, we still do not have a mathematical representation of jet behavior. Summed up honestly by B. Fabre and A. Hirschberg, two of the field's leading investigators, physical models of flue instruments "are based on a strange mixture of ad-hoc assumptions, theories, and fit of experimental results" [3]. My goal is to contribute to alleviating this cacophony of models in addition

to helping to understand the basic science behind fluid motion.

Chapter 2

The History of Acoustics Research

Acoustics, deriving its etymology from the Greek verb *akouein*, to hear, is the science of sound. The passion to understand the production and transmission of sound has driven scientists from the earliest Classical period to the present day to study acoustics. While celestial motion is typically credited as the origin of physics, the same early physicists who spent their nights observing the heavens spent their days examining vibrating strings and probing the science behind music. Pythagoras, best known for his right-triangle theorem and deified status among his followers, believed the roots of mathematics were musical. He discovered certain ratios of tones were more euphonious than others, leading him and his followers to apotheosize musical intervals. Galileo's characterization of a vibrating string contributed enormously to classical mechanics, as he first recognized the relationship between frequency of vibrations and pitch. Daniel Bernoulli, the father of fluid dynamics, worked concurrently on modeling Galileo's vibrating string problem and developing his famous equations describing fluids. Joseph Fourier originally hypothesized that the general shape of any vibrating string could be decomposed into independent modes. He later proved this assertion true, and today physicists use Fourier Series for everything from quantum mechanics to image analysis. More recently, physics greats such as Helmholtz and Rayleigh have devoted significant time to understanding acoustics [4] [5].

Lord Rayleigh published close to 450 papers in his lifetime, of which 128 deal

Figure 2.1: Pythagoras was fascinated with bells and devoted considerable thought to understanding acoustics [6].

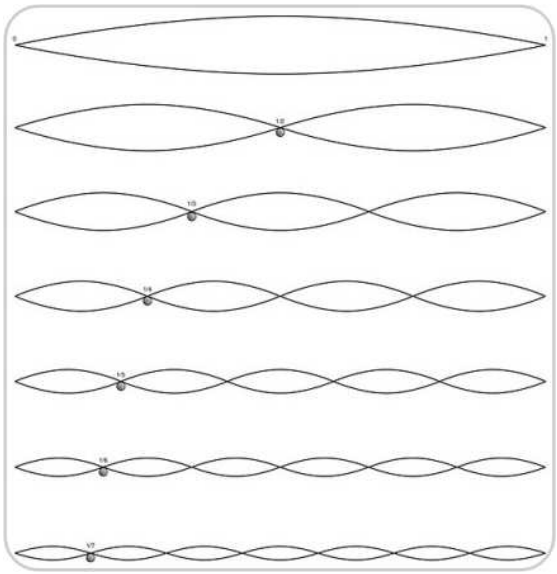

Figure 2.2: Galileo sought to characterize the vibrating string. His quest eluded him and was not completed until centuries later.

with acoustics. Upon these papers, he based his seminal treatise *The Theory of Sound*, which, for the first time, accurately described the production and propagation of sound. He focuses on vibrating strings, bars, and membranes and the propagation of sound through fluids, setting the stage for the modern acoustic research upon which I base my thesis [4].

After World War II, physicists re-discovered flue-instrument acoustics. J. Coltman, A. Benade, and A. Powell focused on qualitatively describing air-jets, edge tones, and resonator tubes [3]. A real breakthrough occurred in 1968 when John Coltman published "Sounding mechanisms in the flute and organ pipe" in *Journal of the Acoustical Society of America*. With this seminal paper he laid the foundation for the next decades of recorder research.

Using a single-channel, sliding-microphone reflectometer, he performed crude reflection measurements off a pressure controlled air-jet. He concluded that the air-jet is a flat, oscillating stream on which the disturbance that excited the resonator propagates at one-half to one-third of the original jet velocity. The disturbance on the jet then strikes the dividing labium. This sharp edge directs approximately half the flow into the fingered resonator tube and half out the window into the air. He showed that this periodicity excites the resonator tube in two different ways. One, later named volume drive and far more important in the actual operation of the recorder, involves the jet entering the resonator at times of pressure minima and injecting actual volume. The second, later called momentum drive, relies on the jet entering the resonator at times of pressure maxima and, rather than the fluid from the air-jet entering the tube, it stops and transfers its momentum. These two drive mechanisms were extensively studied in subsequent research. However, upon further investigation volume drive was shown to be so dominant that momentum drive can essentially be ignored, as it is in this thesis. Finally, Coltman recognized that the air-jet/pipe-resonator system equilibrates within a few milliseconds and settles into a steady-state oscillation frequency dependent on both

the parameters of the resonant pipe and the oscillating air-jet [7].

Neville Fletcher elaborated on Coltman's initial observations in his 1982 paper "Acoustic Admittance of Organ Pipes." While Coltman primarily studied the flute and Fletcher the organ pipe, the mechanism driving both of these instruments is almost identical. Only minor geometric differences separate the recorder and the organ pipe, and research on one is often coupled to research on the other. Thus, Fletcher's examination of the air-jet on the organ pipe is fully applicable to my work on the recorder. Nevertheless, Fletcher attempts to empirically characterize the interaction between the air-jet and the organ pipe using a single microphone reflectometer. He accepts Coltman's assertion that a pipe can be driven by pressure and volume and coins the terms momentum drive and volume drive. Volume drive he defines as injecting fluid into the pipe at points of maximum compression at the driving point. Thus, the oscillating air-jet would inject volume into the pipe in phase with its driven frequency. That is, as the jet whipped below the labium a running pressure wave would just be reflected off the open end of the mouth of the recorder and the air-jet would increase its amplitude.

Later research has shown volume drive is primarily responsible for sound production in the recorder and my measurements show that extremely low pressure and fast flow rates drive the instrument are consistent with that assertion. Momentum drive, however, cannot be totally discounted. It is defined as the jet slowing down and transferring its momentum to the oscillating running wave thereby increasing its amplitude. In the momentum drive mechanism the jet does not continue down the pipe, but rather just pushes the oscillating wave at its resonance like pushing someone on a swing. Although momentum drive makes a fairly small contribution to sound production in the recorder, reed-driven instruments like the clarinet are primarily driven by this mechanism. Interesting to note, momentum drive and volume drive are $\frac{\pi}{2}$ out of phase. Because flow is maximized where pressure is zero and a maximum pressure leads to a minimum flow, at a blocked end for example, this out of phase behavior makes sense.

The latest recorder research has been done by Marc-Pierre Verge, Patricio de la Cuadra, A. Hirschberg, and B. Fabre. Much of their work relies on Schlieren imaging, a technique in which a gas with an index of refraction different than air is passed through the system and imaged using special optical techniques. This visualization allows many of the rough original models proposed by Fletcher and Coltman to be verified [8]. Because this newer technique allows the researchers to actually visualize the jet, they are discovering that many aspects of flue instruments are not as mathematically simple as originally thought and that new elements previously disregarded, such a vortex shedding, play a role in sound production. For example, Fletcher's model assumed that saturation, that is maximum sound amplitude, would be reached due to radiation and viscous wall loses. Schlieren imaging, however, has shown that the shedding of vortices off the jet is responsible for far more energy loss than either radiation or wall loses [9]. In addition, non-linear behavior, attack transients, and other subjects beyond the scope of this thesis have been studied to a degree of detail impossible with previous experiments.

The AVNA, described in the next chapter, is yet another tool designed to accurately study these questions and my research should provide another perspective that can be compared to that already published.

Chapter 3

The Acoustic Vector Network Analyzer (AVNA)

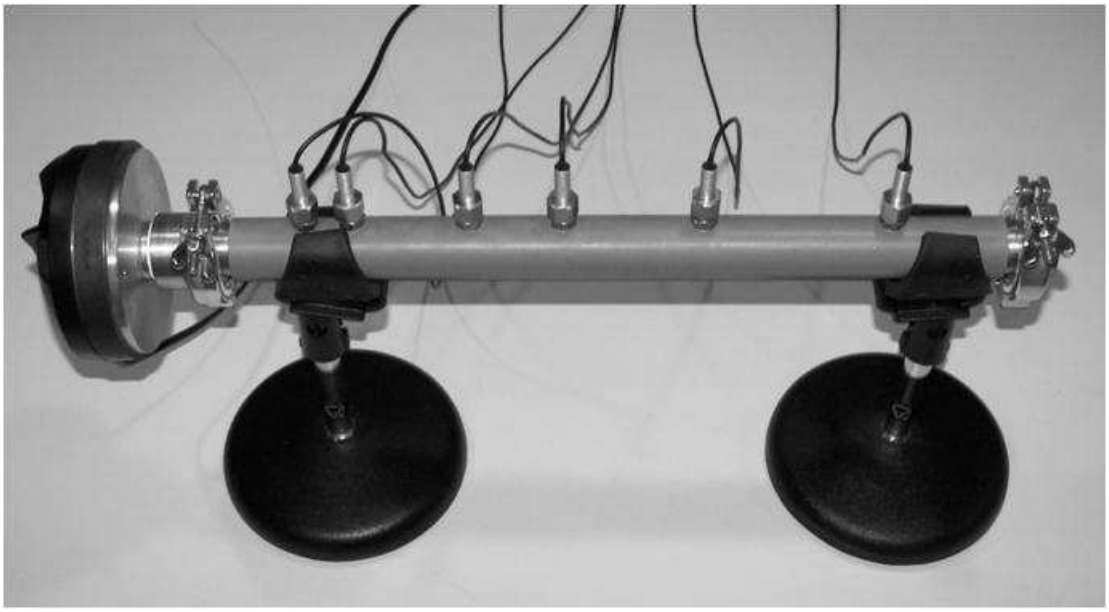

Figure 3.1: The AVNA is a cylindrical waveguide bored out to the exact inside diameter of a plastic Yamaha tenor recorder. The microphones sit flush with the inside of the tube and are spaced to minimize the chance of nodes or antinodes falling on multiple microphones. All six microphones are simultaneously sampled by a PreSonus FP10.

The AVNA consists of a compression driver coupled to a cylindrical waveguide bored out to the same inside diameter as the head joint of a plastic Yamaha tenor recorder. Six microphones, whose sporadic placement was determined by a Monte-Carlo simulation, are fitted along the guide and mounted with their ends flush to the inside of the tube, as not to disturb the wave, collect the data via a recording interface

that simultaneously samples all six signals. In essence, the AVNA is an extension of the sliding, single-microphone apparatus used by Fletcher and Coltmann. While acoustics researchers in the 1960's were limited by technology at the time, the PreSonus FP10 that our group uses simultaneously samples six signals and is available for only $400. Using six relatively-calibrated microphones flush with the guide eliminates many of the problems faced by earlier researchers, especially the issue of the microphone disturbing the acoustic field. Figure 3.2 shows the apparatus Fletcher used for his 1983 *Journal of the Acoustic Society of America* paper "Acoustic Admittance of Organ Pipe Jets".

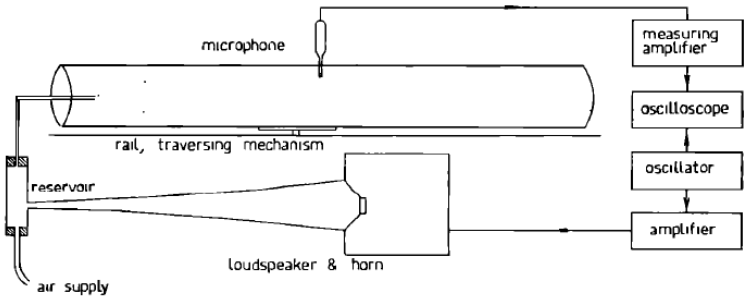

Figure 3.2: Fletcher used a device that could be described as a single-microphone AVNA for some of his experiments [10].

When the AVNA is driven by our Selenium D210TI compression driver, the microphone diaphragms are variably compressed through time changing their internal capacitances and forming a potential. These electric signals are simultaneously collected by the FP10 and imported into MATLAB as a set of complex amplitudes, phasors, that encapsulate both amplitude and phase relative to the first microphone. Figure 3.3 helps to visualize how these complex amplitudes are collected. Usually I drive the AVNA over a range of frequencies to explore frequency specific behavior giving MATLAB relative phasors as a function of frequency. From the raw phasors, my MATLAB routine assumes that only a left- and right-going wave exist in the guide and that attenuation and phase velocity smoothly vary with frequency, based on Arthur Benade's 1968 model

[11]. The data are sorted into MATLAB's nonlinear least-squares fitting routine, which iteratively calculates left- and right-going complex amplitudes and compares calculated phasors at the actual microphone positions. The waves calculated are of the form

$$Ae^{i(\frac{\omega}{v_p}-i\alpha)x_r} \tag{3.1}$$

where A is the complex amplitude, ω is the angular frequency of excitation, v_p and α are the phase velocity and attenuation calculated using Benade's model, and x_r is the user-defined reference plane. Figure 3.4 shows the high accuracy of the calculations. The recorded phasors are off by less than one part in ten thousand. Once the routine settles on left- and right-going waves that accurately describe the collected phasors, I calculate the reflection coefficient by simply dividing the reflected wave by the incident wave as in Equation 3.2 where W_r and W_i are the reflected and incident wave equations.

$$\Gamma = \frac{W_r}{W_i} \tag{3.2}$$

While much of the previous recorder research has focused on acoustic impedance rather than reflection coefficient, I chose to work with reflection coefficient because it is much easier to visualize and, with a little algebraic manipulation, can be converted into more familiar values. In essence, reflection coefficients allow me to most easily examine how an air-jet affects an incident wave.

As simple as this process sounds, a significant amount of calibration is required before meaningful data can be produced. Some acoustics labs use expensive laboratory microphones that are absolutely calibrated, that is a given pressure will result in a defined signal. Our lab, however, believed that equally good data could be collected from cheaper microphones that could be calibrated relative to each other. This choice is strongly supported by the data, but the calibration routine is essential. Given the inexpensive diaphragms our lab uses vary by up to 5 dB, any microphone abnormality has to be removed else the extremely precise data collected by the AVNA would be

useless. Figure 3.6 shows raw data collected with one dramatically less sensitive microphone. I fixed the problem for consistency's sake, but the calibration routine had no problem correcting for the bad microphone. To overcome these differences in sensitivity our group machined a calibration cell that mates to the driver and holds all six microphones equidistant from it as shown in Figure 3.7. The MATLAB code then sounds the driver for a $\frac{1}{2}$ second through a range of user defined range of useful frequencies[1] at constant amplitude. The end product of the calibration process is a file detailing the exact differences in microphone sensitivity and is encapsulated in Figure 3.8. The data collecting routines call that calibration file and software-correct the values for each microphone given their physical differences. However, the calibration process does not solely rely on software correction. The FP10 has volume adjustment knobs for each channel. Before using a calibration file, I would do my best to correct out microphone differences at the hardware level.

Once the microphones were calibrated, I tried to start collecting meaningful data. However, I had to address one more concern. Initially we were concerned that the microphone calibration might drift during the course of the experiment, given we use inexpensive off-the-shelf components rather than research grade acoustics equipment. This fear was allayed by simply recalibrating the microphones several times over long periods of time and comparing the calibration files. It turns out that the drift is negligible, about $\frac{1}{10}\%$ in amplitude and $\frac{1}{100}\%$ in phase. Figure 3.9 displays the percentage change over different frequencies.

After calibrating and checking for microphone drift, I need to run a few simple experiments, all pictured in Figure 3.11 to assure myself that the AVNA actually works. While analytical fluid mechanics is difficult and exact solutions only exist for a few simple problems, I can duplicate a few of these simple situations and check to see that

[1] When studying recorder behavior I scanned through the lower octave playable on the tenor recorder; from C4 to C5 or from 250 Hz to 1200 Hz.

the AVNA data agree with the analytical solution. A tube with a closed end should have a reflection coefficient of exactly one as radiation is impossible and attenuation is minimal. Likewise, the reflected wave should be in phase. Thus, with one end of the waveguide blocked off, I should find reflection coefficient to be one and phase to be zero over all frequencies. Fortunately, I produced those results. Figure 3.12 provides an indication of error and shows that the AVNA falls within 1% or so of theory in both phase and amplitude.

Another well-characterized situation is an open end. Unfortunately, at least for the purpose of this experiment, the AVNA has a small flange and is not a perfect open end, but it is close enough. Assuming the wavelength of the wave within the waveguide is much longer than the open aperture, it will be reflected with 100% efficiency out of phase. Thus, at low frequencies, I would expect to see a reflection coefficient of one and a phase of π, while at higher frequencies I would expect some radiation leading to a reflection coefficient of less than one. Figure 3.13 shows the reflection results from an open end experiment. While not quite as precise as the closed end, they mirror theory quite while and the relative inaccuracy could be easily chalked up to the physical situation. Also interesting to note is that the reference plane for the open is set six millimeters longer than that of the closed end because of end correction effects, that is the effective length of the pipe grows. These end corrections are essential in the correct tuning in any open end flue instrument.

Finally, I can test radiation behavior with a horn. An ideal horn would reflect all frequencies below its cutoff and radiate all above. Our lab bought a HL14-15 horn with a 600 Hz cutoff. Figure 3.14 shows that the horn behaves properly and the HL14-15 radiates much better above 600 Hz.

These three idealized physical situations provide evidence that the AVNA works as it should. With evidence that my data closely matched analytical calculations, I felt confident I could go on to use this apparatus to study the recorder.

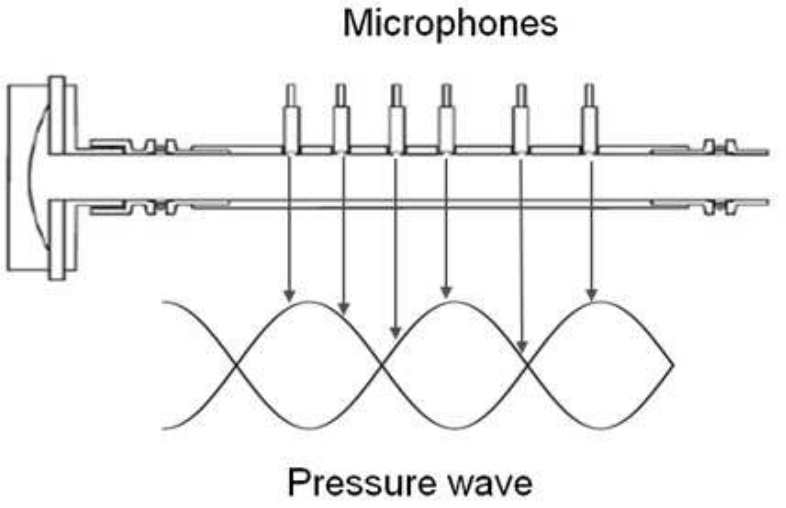

Figure 3.3: The pressure wave within the guide depresses the microphone diaphragms creating an electric signal from which our MATLAB routine constructs left- and right-going waves [12]

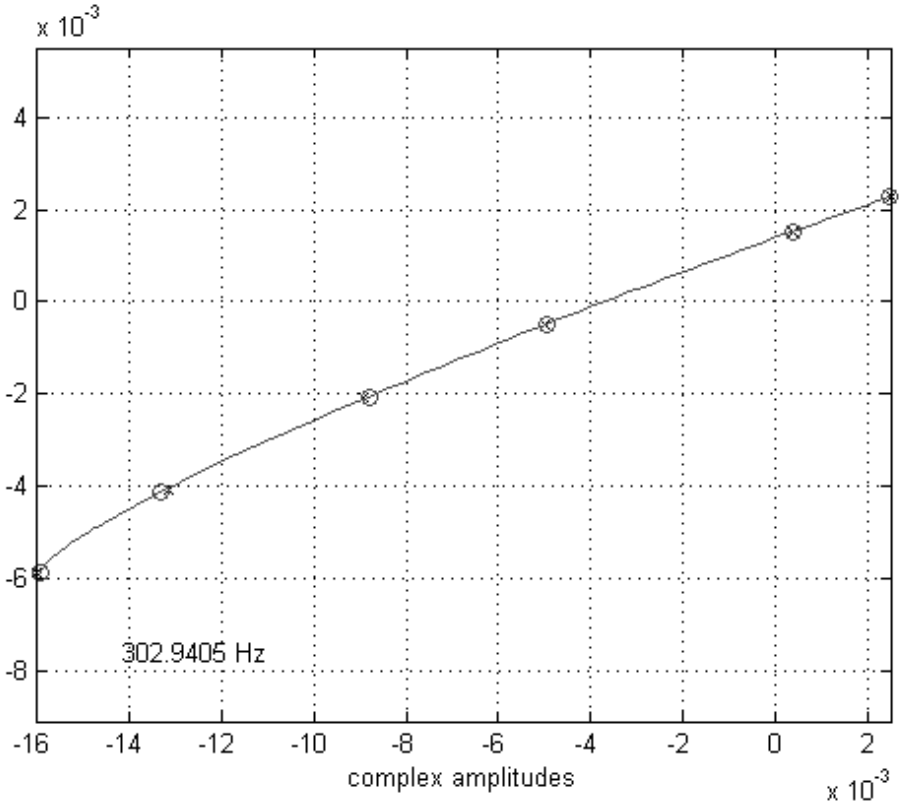

Figure 3.4: The small x's are the actual phasors measured by all six microphones at 303 Hz and the red dots are those predicted by the fit. This routine is very accurate as evidenced by the scale. These data come from the recorder head being blown at 88.2 Pa.

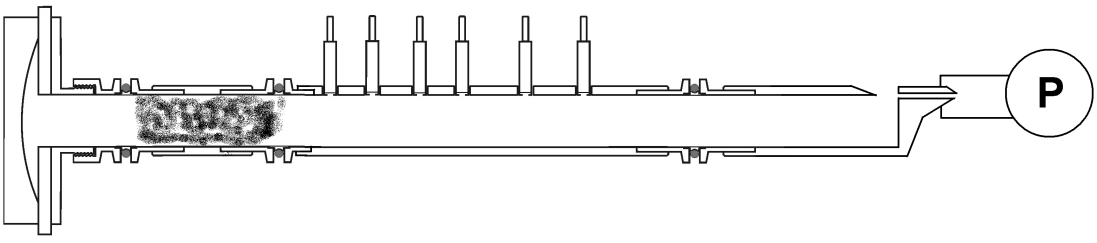

Figure 3.5: The recorder head is mounted on the end of the AVNA with a controlled pressure source, labeled P, driving the air-jet. The speckled section between the driver and the microphone section is the cotton attenuator necessary to prevent multiple incident and reflected waves.

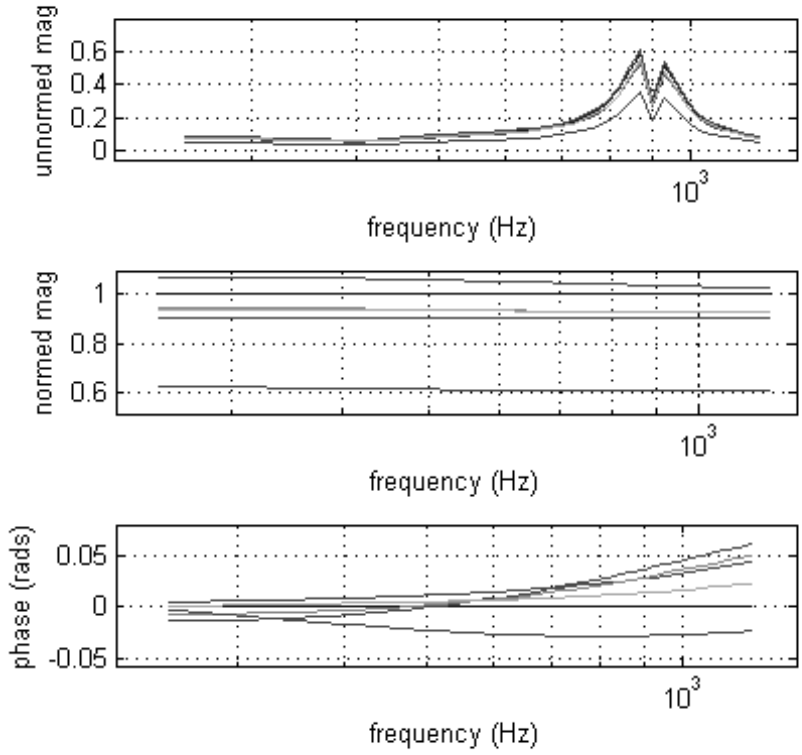

Figure 3.6: These data show the consequences of a bad microphone. Here mic 4 is roughly 40% low in amplitude and 10% off in phase. This particular abnormality was caused by a small particle on the diaphragm rather than a software error, but, even with the enormous correction factor, the data I collected using this calibration file looked fine.

Figure 3.7: The calibration cell holds all six microphones equidistant from the driver. The driver runs through user-defined frequencies at a constant amplitude while the PreSonus collects phasors. These data allow MATLAB to correct for differences in microphone sensistivity.

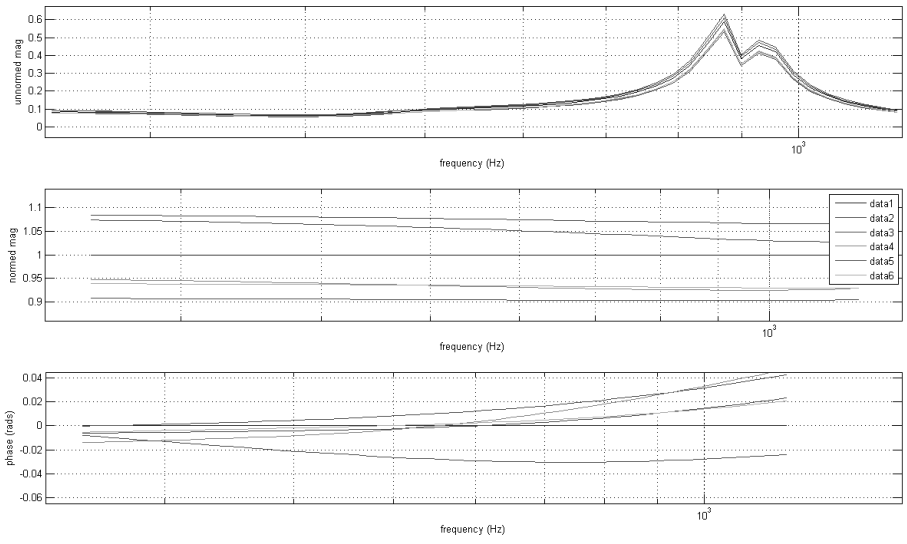

Figure 3.8: This is the calibration cell file I used as a standard comparison and one which I ran many experiments. Out of the box the microphones vary around 15% and the correction factors are shown in the normed mag plot.

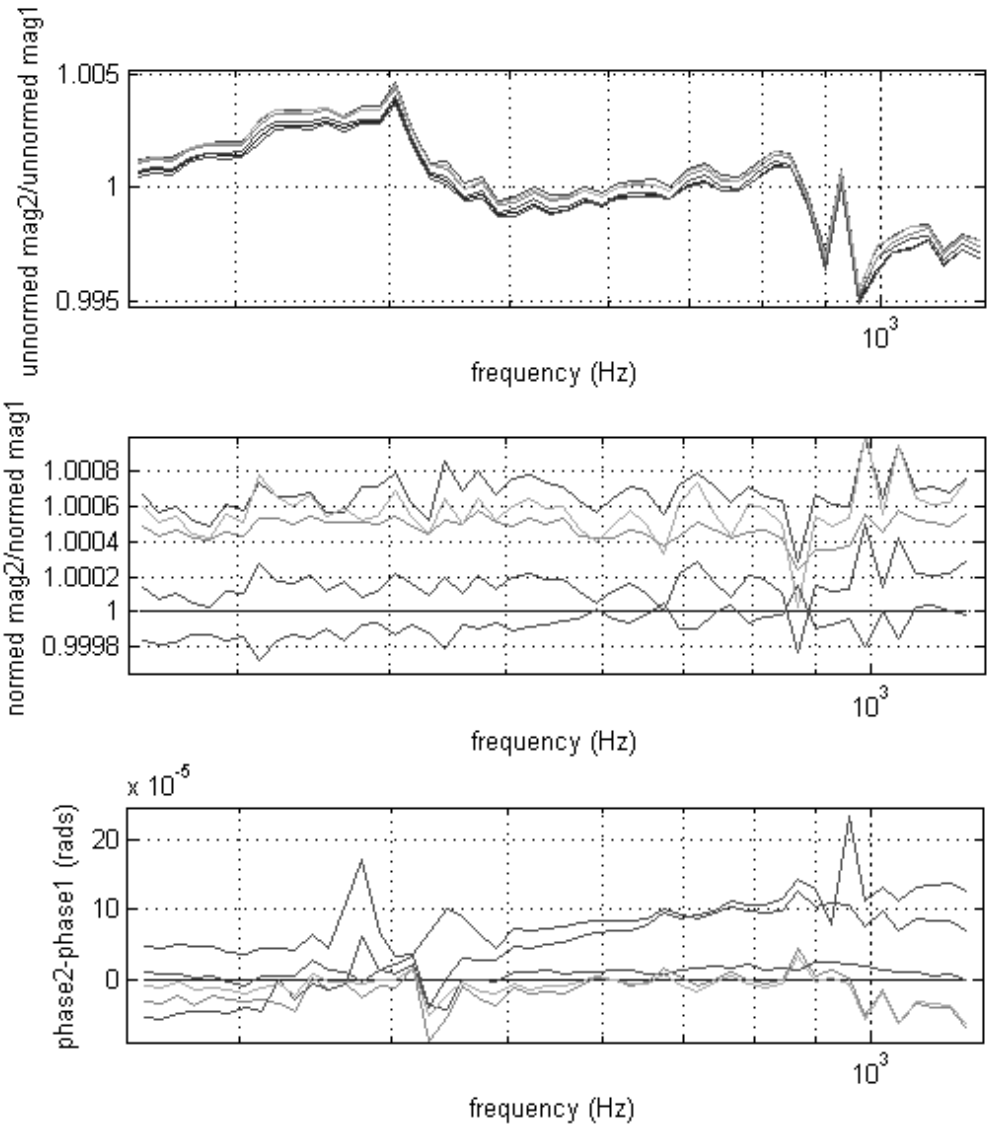

Figure 3.9: Shown are the calibration cell recorded phasors approximately 24 hours apart. Despite their small price tag, the microphones used drift an inconsequential amount. This table would look almost identical after even six months and most of the small changes can be attribute to error rather than microphone drift.

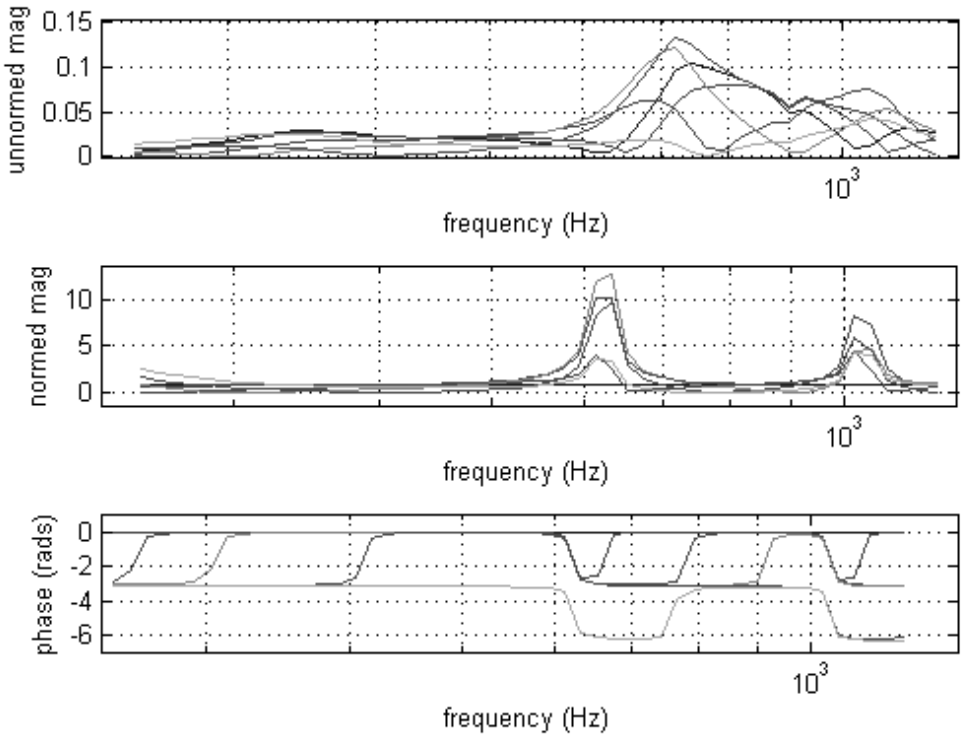

Figure 3.10: The closed end raw data look like this. Each line represents a microphone and the subplots track their relative phase and amplitude through frequency. This plot already provides some idea of wave within the guide. We can see that at higher frequencies the microphones' amplitudes increase, demonstrating that once the wavelength gets short enough, there is a strong chance of a wave anti-node falling exactly on a microphone.

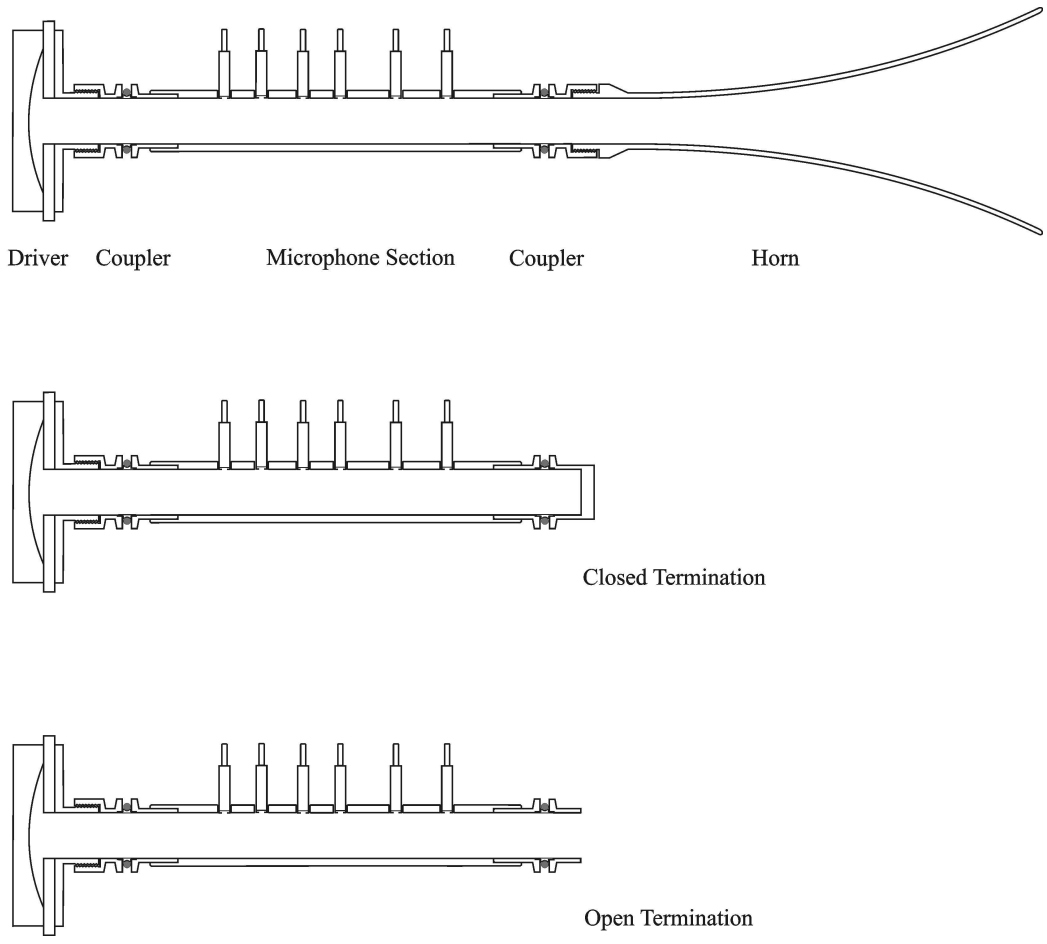

Figure 3.11: The horn, closed end, and open end are all well characterized and provide a check on the function of the AVNA [13].

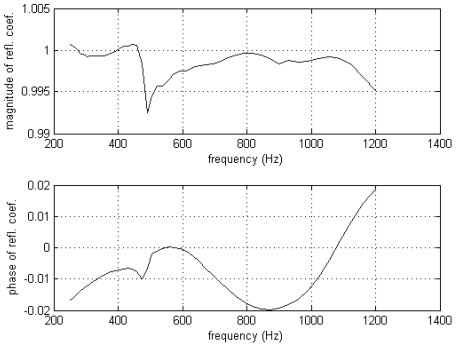

(a) Reflection coefficient amplitude and phase separated

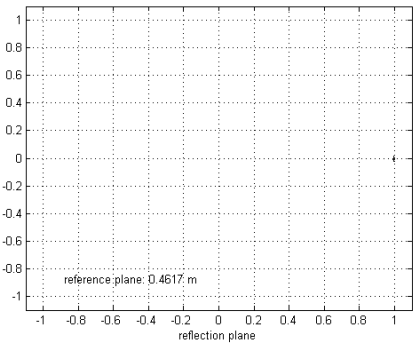

(b) Reflection coefficient on complex plane

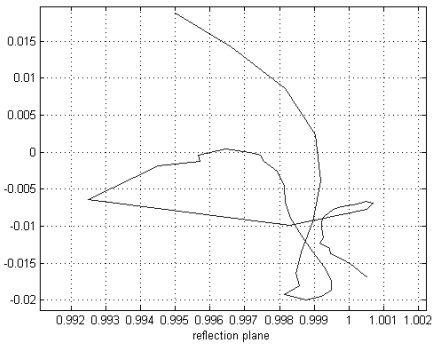

(c) Reflection coefficient of complex plane centered on data

Figure 3.12: There are two equivalent ways of presenting reflection coefficient data, in the case reflection off a closed end. The first, as seen in Subfigure (a), is easy to understand and shows the phase and amplitude of the reflection coefficient separately as functions of frequency. The second uses a complex plane. The distance from the origin is the magnitude of the reflection coefficient and the angle between the positive x-axis and the point is the phase. Subfigure (b) shows the entire plane and the cluster of points is just visible at (1,0) while Subfigure (c) gives an indication of precision.

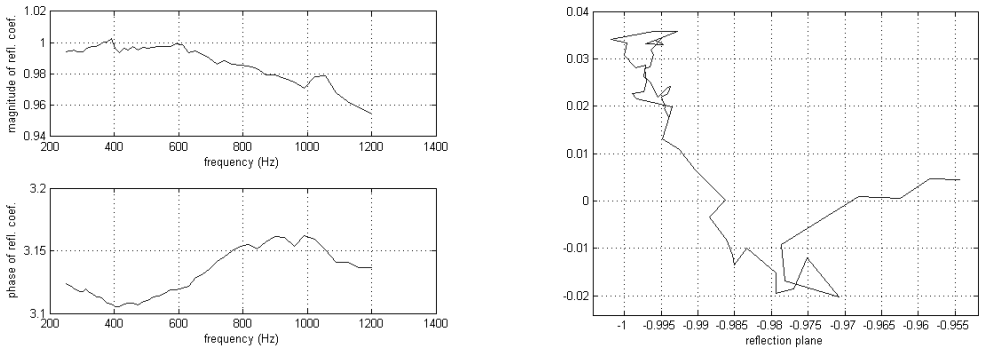

(a) Open end reflection coefficients

(b) Open end reflection coefficients in the complex plane

Figure 3.13: The open end clearly is not as useful a metric as the closed end, but the predicted behavior is visible. At higher frequencies the pipe begins to radiate and at lower frequencies the reflection coefficient sits around (-1,0) on the complex plane.

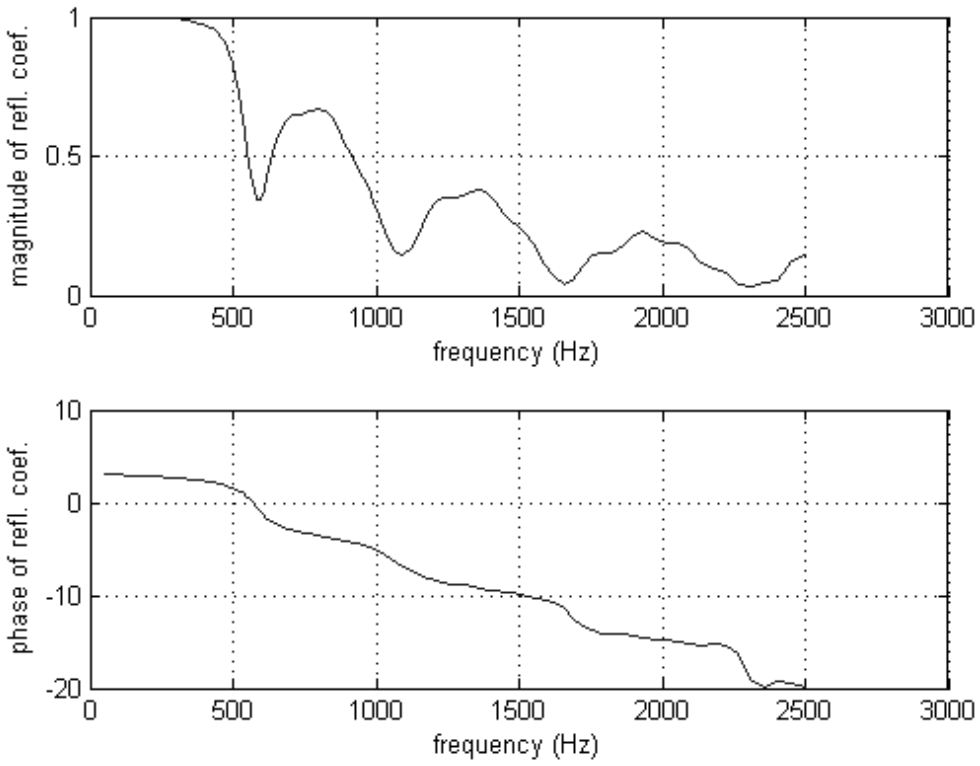

Figure 3.14: The 600 Hz horn starts radiating at around 600 Hz. Some kind of resonance exists at 600 Hz and the higher frequency harmonics, causing the periodic dips in reflection coefficient.

Chapter 4

Review of Lumped Element Models

When approaching a new problem, it is necessary to settle on a level of complexity detailed enough to provide enough understanding to answer the questions being asked, but not so detailed as to burden the researcher with unnecessary complications. For example, to return to the engineer assigned to design a new engine for Yamaha, he cannot study internal combustion from the perspective of a black box in which fuel is converted to work, but he also cannot examine the electron orbital interactions of every atom. The same complexity versus practicality concern arises in the study of the recorder. There are two real schools of thought. One, called the integral approach, involves approaching the assembled recorder as a black box of sorts in which an experimentalist can control air flow or pressure into the mouthpiece and fingering and measure the resulting acoustic spectrum. Figure 4.2 shows a simple integral experiment. Volume flow, and thus blowing pressure, is varied for three different fingerings and the frequency of the strongest fundamental is measured. Through this experiment, I confirmed suspicions that frequency rises with blowing pressure for a given fingering and that, given the right conditions, a note can be overblown to the next octave. Aside from such simple conclusions, studying the recorder through integral methods is extremely difficult. More information can be teased out of a complete power spectrum, but designing a productive experiment that isolates one variable still challenges scientists. If, for example, I attached the entire assembled recorder to the end of the AVNA to try to determine some

kind of behavior I would run into multiple incident and reflected waves. After summing the waves, I would find that the incident wave is no longer linearly related to the reflected wave. Rather , when the system is spontaneously oscillating, an incident wave can exist without the presence of a reflected one and vice-versa. Taking reflection data for an oscillating system is therefore meaningless. Just for fun, I mounted the recorder head onto the end of the AVNA without the attenuator inline and took "reflection data" while the system was oscillating to see what kind of phasors the MatLAB routine would find. Figure 4.1 shows that the calculated phasors are nowhere near the actual values and convinced me that I had to be very careful to throw out any data points taken when the system demonstrated even the slightest hint of spontaneous oscillation. However, when the attenuator is properly packed and mounted inline, the reflected wave is linearly dependent on the incident one[1] , allowing me to take meaningful reflection data.

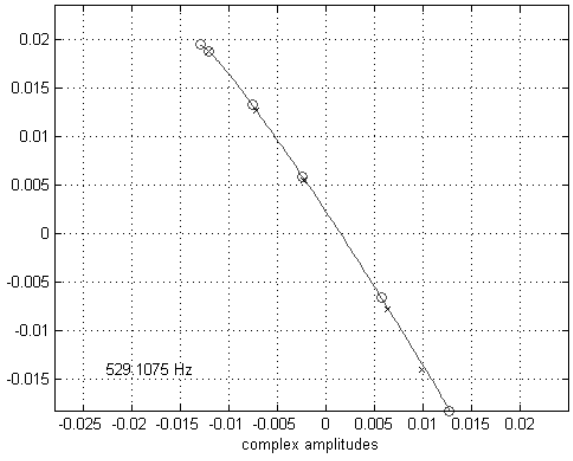

Figure 4.1: When the system is allowed to spontaneously oscillate, the reflected wave is no longer linearly dependent on the incident one. The ideas of reflection coefficient and calculated right- and left-going waves are rendered meaningless. These calculated phasors, taken without the crucial attenuator in place, totally miss their marks.

[1] Once the incident wave amplitude gets closer to saturating the instrument, reflection off the air-jet becomes non-linear, but all my experiments were solidly in the linear region.

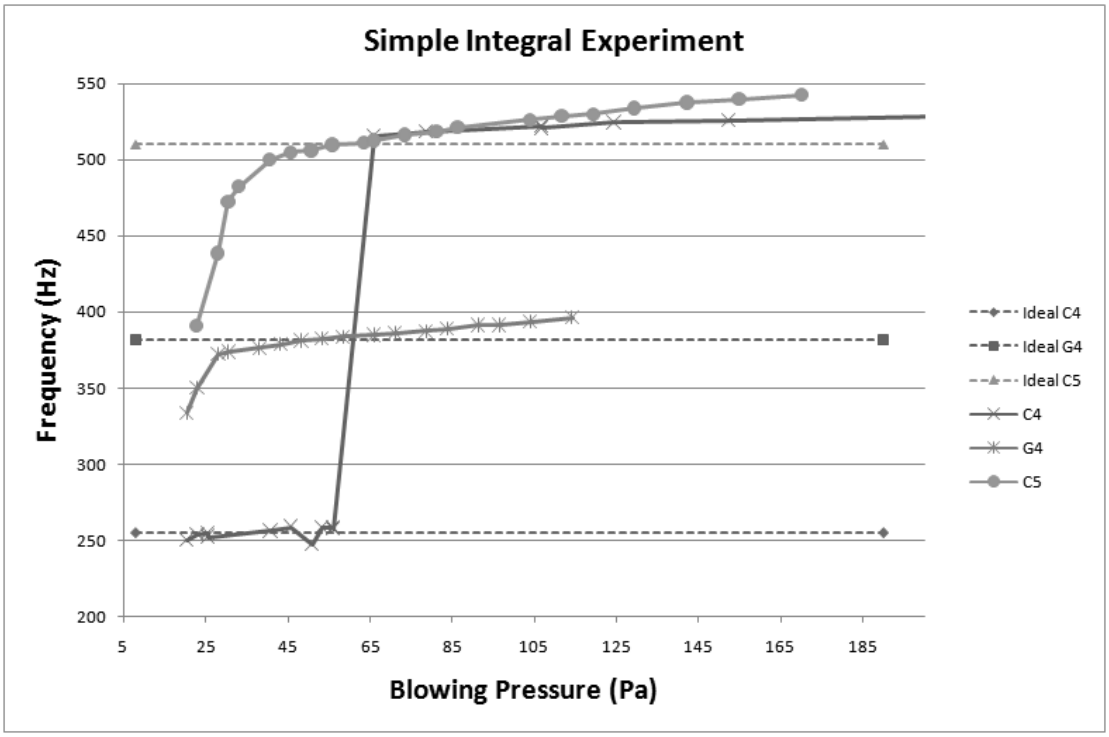

Figure 4.2: Here the recorder is assembled and fingered to blow either a C4 (261 Hz), a G4 (392 Hz), or a C5 (523 Hz) and the actual frequency radiated is plotted as a function of blowing pressure. In this plot the dotted lines show ideal values and have been lowered to compensate for the colder-than-body-temperature air exciting the instrument.

Instead, despite complaints from some acoustics researchers that lumped-element models provide an overly simplistic model, I decided to separate the recorder into two distinct elements: the fingered pipe resonator and the air-jet amplifier [3]. Since the reflected wave from the pipe clearly must be both in phase and match amplitude with the incident wave on the jet, I ideally could combine data obtained from each end separately to form an integral model. While I did not get far enough in my research to construct a model, I make several interesting observations about both the mouth and the body that in the future could be combined.

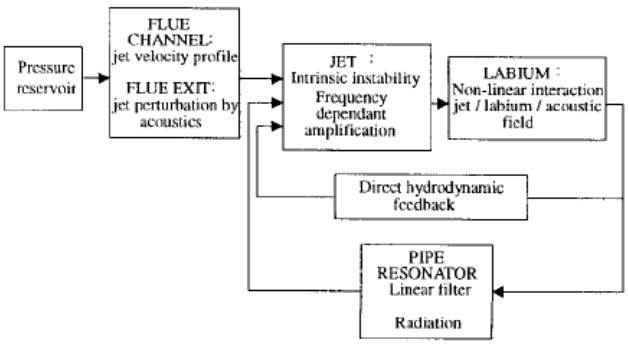

Figure 4.3: A sample diagram representing the different elements of a recorder. Depending on the level of sophistication of the model some of these may be absent or ignored [3].

Figure 4.4: This project assumes two simplified elements: an air-jet amplifier and an acoustic resonator.

Chapter 5

The Mechanics of a Recorder

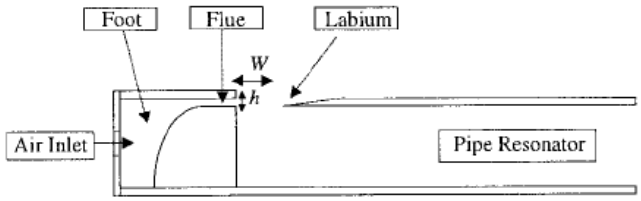

Figure 5.1: Shown here is a simple cutaway diagram of the recorder head. Recorders typically have a $\frac{W}{h}$ ratio of 4 while organ pipes are closer to 10. This affects the degree of turbulence that hits the labium [3].

A recorder belongs to a family of flue instruments that includes the transverse flute, the organ, the whistle, and many others [3]. Its basic principle of operation is as follows: a pressure source drives air through the flue and it exits the mouth to become an air-jet. As Rayleigh proved in the second volume of *The Theory of Sound*, that air-jet is intrinsically unstable and begins to oscillate [14]. The oscillating jet next encounters the labium, a sharp divider that may or may not be placed at the equilibrium point of the air-jet. The labium splits the jet forcing approximately half of its volume to exit the instrument through the duct and injecting the other half into the pipe resonator with some periodicity. Because the mouth and body of the recorder are coupled, the jet injects into the pipe resonator in phase with its internal oscillation that determines the frequency of the note played. That is, as the wave in the pipe resonator begins to

pulse in, the air-jet injects to amplify its signal. Figures 7.9 through 7.13, taken through Schlieren imagery techniques, help visualize the motion of the air-jet a different blowing pressures.

As discussed earlier, there are two possible drive mechanisms for a flue-instrument. One, called momentum drive by Fletcher, relied on the momentum of the air-jet for energy transfer to the pipe resonator. In this situation to achieve maximum efficiency the air-jet would come to a stop at the entrance to the pipe and transfer all of its momentum to oscillating fluid inside. A more familiar example of momentum drive can be seen in a wind turbine. The momentum of the wind is transferred very efficiency to the blades and slows down significantly by the time it reaches the other side. The other possible drive mechanism Fletcher calls volume drive. In this scenario the volume flow from the jet enters the pipe at the time of maximum compression and serves to amplify the signal. Because momentum drive occurs at times of maximum fluid velocity and volume drive occurs at times of maximum compression, they are $\frac{\pi}{2}$ out of phase and both contribute [10]. In order to understand which mode dominates the interactions in a recorder, researchers have performed several experiments to try to isolate the modes. One clever one, done by Coltman in 1981, involved varying the directionality of the jet while injecting at the middle of the pipe [15]. Coltman reasoned that momentum drive is direction, that is changing the direction of momentum should change the phase by π, while volume drive is a scalar interaction and a shift in direction should not affect the phase.

Chapter 6

Experimental Procedure

After checking microphone calibration and ensuring that the closed end measurements remained within 1% in both amplitude and phase, I set up my recorder experiment. First, I had to settle on a standard reference plane. Two obvious ones sprang to mind. I could either set the reflection plane at 0.643 meters, the point at which the recorder head behaves most similarly to an open end, or I could set it 0.462 meters, the plane at which the recorder contacts the wave guide. In the end I could not find an advantage to using one over the other and eventually settled on the 0.462 meter number. If later I find that I would like to reanalyze my data at the pseudo open end, it is a simple MatLAB procedure to switch.

Next, I had to make sure that my attenuator functioned over most useful frequencies. As discussed before, it is essential to place a short attenuator tube in between the driver and the microphone section to avoid multiple left- and right-going waves. The MatLAB code running the AVNA is setup to assume one left-going and one right-going wave. If the incident wave, from the driver, were allowed to reach the air-jet, get amplified and reflected, and re-reflected at the driver end, I would end up with an oscillating system with multiple incident and reflected waves. Figure 4.1 demonstrates that no useful data can be attained from an oscillating system. Thus, I needed an attenuator that would absorb fairly flatly over all frequencies. This proved to be quite difficult as a harder attenuators that absorbed better at some frequencies tended to reflect at others

and softer attenuators absorbed at some, but transmitted at others. Fortunately, I was aided by the fact that a sound wave only must pass through the attenuator once on the way to the jet, but must pass twice in order to be reflected effectively doubling the length of the attenuator where I really needed it. In the end, after experimenting with several materials, I settled on lightly balled cotton. Figure 6.1 demonstrates cotton's frequency dependent attenuation characteristics. While certainly not flat, it succeeded in preventing the system from oscillating over most frequencies. While the reflection data show around a 90% attenuation factor, I had to make sure that was good enough with a simple experiment. To ensure I had a good attenuator, I needed to only slowly increase the blowing pressure while listening carefully for sound. Aside from wispy, high-pitched edge tones, a non-oscillating system should be silent. If I heard the beginnings of a note, I knew I had to either repack my attenuator or ignore the data from that blowing pressure. In the end, I learned that cotton just does not attenuate enough around the 800 to 1200 Hertz region, depending on the pack, and I discarded the tainted data.

After totally preparing the apparatus, I was prepared to begin the experiment. Because I was interested in the reflection off the jet over different frequencies at different blowing pressures, I had to run through a number of variables. I would slowly, by approximately 1 Pa each step, measuring pressure with a Dwyer Series 475 Digital Manometer, ramp up the blowing pressure and sound the driver from 250 to 1200 Hertz, taking reflection data at each frequency producing a series of plots of frequency versus reflection coefficient. These graphs allowed me to examine how blowing pressure affects the reflection coefficient at different frequencies. Figure 7.2 shows the finished plot.

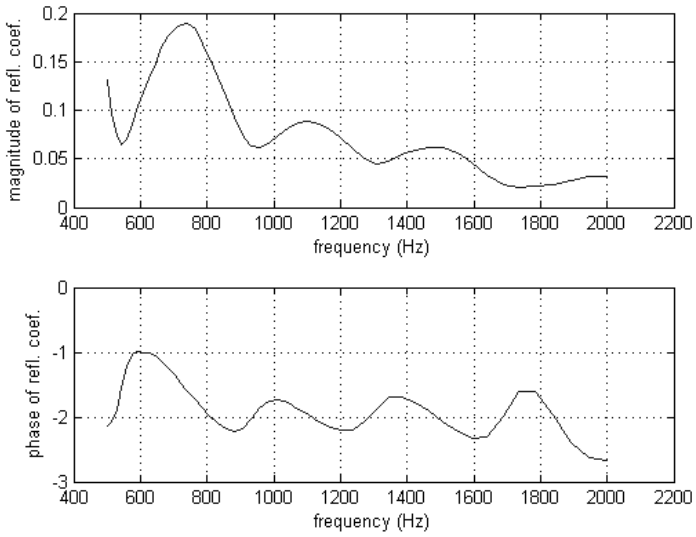

Figure 6.1: The attenuator's behavior over frequency is not flat, but kept the system from oscillating over most blowing pressures. In the regions around the peak at 800 Hz, the system would occasionally sound and I would discard those data.

Chapter 7

Results & Discussion

The results from my first experiment were quite promising. I knew from my earlier integral experiment shown in Figure 4.2 that a blowing pressure of approximately 56 Pa was needed to properly sound a 523 Hz C5, 50 Pa a 392 Hz G4, and 25 Pa a 261 Hz C4, also known as middle C. This suggested that a higher blowing pressure is needed to sound higher notes and my data demonstrated this trend remarkably. Even more interesting was the fact that at about 32 Pa the reflection coefficient maximum is at 270 Hz, at 50 Pa it is at 390 Hz, and at 56 Pa it is at 450 Hz once corrections are made for air temperature. One would assume that the instrument would sound at approximately the same frequency as the reflection maximum of the air-jet, and these numbers support that trend.

After running one very careful experiment, the results seemed too good to be true so I waited about a month and, under identical conditions, reran. Fortunately, I was able to reproduce everything from one experiment to the next. The locations and magnitudes of the reflection peaks stayed very stable as shown in Figure 7.1 and even the shapes and small dips remained consistent. Figure 7.2 shows several of the frequency versus magnitude of reflection coefficient plots at different pressures from my second experiment. The data from the first experiment are nearly identical so are not shown.

After obtaining frequency dependent data, I had to somehow compare my work

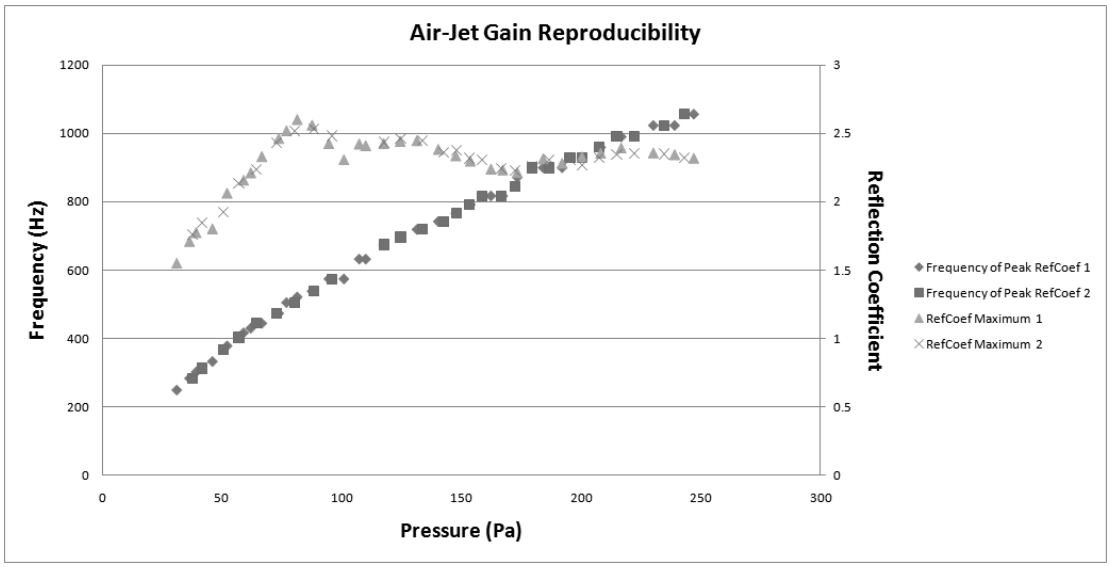

Figure 7.1: Plotted are the magnitudes of the maximum reflection coefficients at different blowing pressures and the frequencies at which they are located for two different experiments a month apart. The plots fall almost right on top of each other showing strong reproducibility. The attenuator failed and the system started sounding for several pressures so some points are omitted.

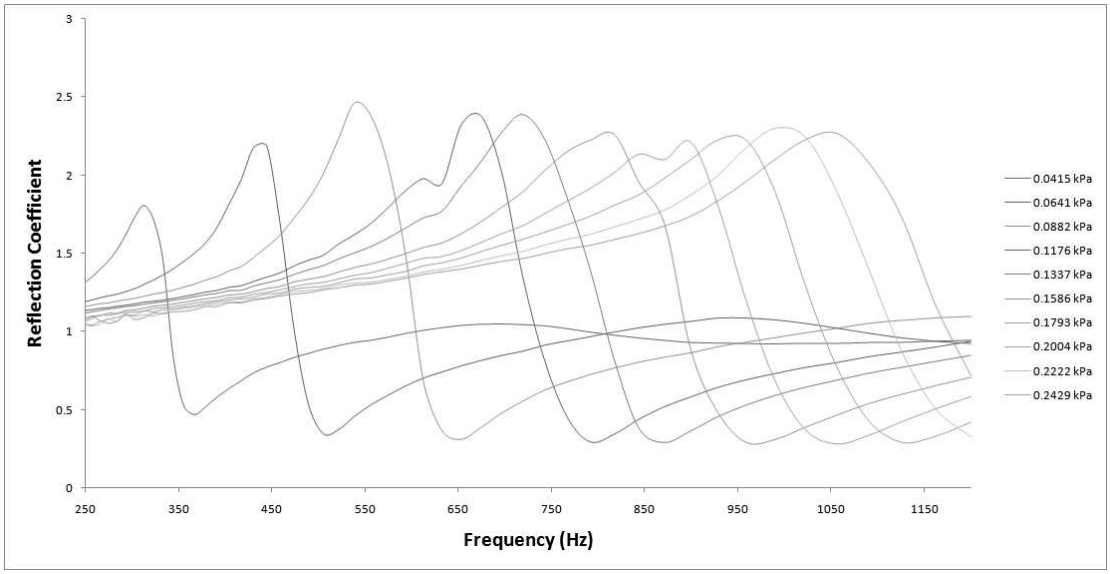

Figure 7.2: The maximum reflection coefficient smoothly moves to higher frequencies as the blowing pressure increases. This explains why a musician must blow harder to sound higher notes.

to that done previously. Ideally, I would take reflection data from the fingered end and somehow combine everything into an elegant model using boundary conditions, but the hodge-podge of competing models and techniques made it difficult to understand where to start. Instead, after reading M.P. Verge's and P. De La Caudra's theses, I focused in on a dimensionless quantity called the Strouhal number that would more accurately describe the physical situation [9] [8]. The Strouhal number

$$St_W = \frac{fW}{U_j} \tag{7.1}$$

takes into account the frequency of the disturbance[1] , f, , the speed of the jet U_j, and the distance from the mouth to the labium, W, which is 4.80 millimeters for a Yamaha tenor recorder (see Figure 5.1). In essence it is half the number of wavelengths on the jet that fit between the mouth and the labium because the disturbance on the jet travels at about half the jet speed [16]. The relationship between the propagation speed of the disturbance and the jet velocity is quite complicated and can only be solved numerically, but Figure 7.3 from *The Physics of Musical Instruments* shows that when kb, the wave number times the half-width of the jet ($\frac{h}{2}$ in Figure 5.1), equals one, as is approximately true with the tenor recorder at most frequencies,

$$\frac{u}{U_j} = \frac{1}{2} \tag{7.2}$$

where u is the propigation speed of the disturbance on the jet [16].

Given I would like to represent my data with the Strouhal number as the independent variable as to anchor them to a concrete physical situation, I needed to collect all the elements involved. I knew the frequency of the disturbance, so I needed W and the jet velocity. W I simply measured with a machinist's feeler gauge to be 4.80 mm[2] .

[1] In the case of an assembled recorder, the acoustic oscillation inside the fingered section is the disturbance frequency, but in the case of my experiment it is the frequency at which I drive the AVNA.

[2] For those interested in where the Yamaha tenor recorder falls on the $\frac{W}{h}$ spectrum, I measured h to be 0.80 mm, yielding a ratio of 6. This is above the 4 idealized for a recorder, but below the 10 idealized for the organ by Verge [9]. This means the jet of this tenor recorder is more turbulent than a

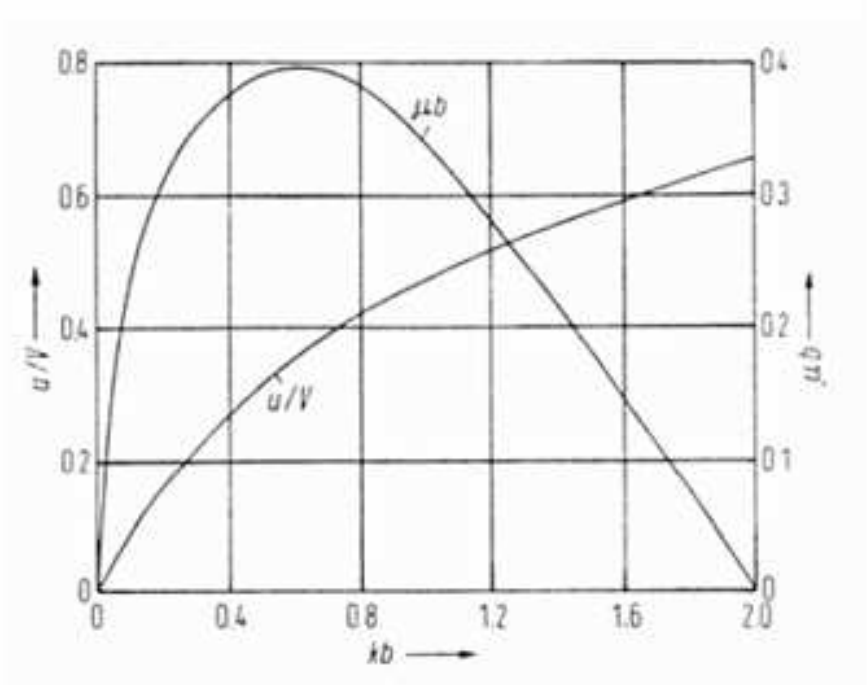

Figure 7.3: This numerical solution shows the dependence of the propagation speed of the disturbance, u, divided by the jet velocity, V, on half of the jet width, b times the wave number of the perturbation, k. The other line shows the dependence of the growth factor and is not entirely relevant to this thesis. In the region around $kb = 1$ where the tenor recorder usually operates, $\frac{u}{V}$ (U_j is also referred to as V in some literature) varies very slowly, so it is possible to roughly approximate the propagation speed as half the jet velocity [16].

Finding the jet velocity would not be so simple.

Daniel Bernoulli found that

$$U_j = \sqrt{\frac{2p_0}{\rho}} \tag{7.3}$$

where U_j is the jet velocity, p_0 is the pressure drop, and ρ is the fluid density, in 1738 in *Hydrodynamica* [17]. In an ideal world, this would be a perfectly accurate way to calculate jet velocity and is used in much of the literature to represent the maximum velocity. Because Bernoulli neglects the energy-robbing effects of viscosity and compressibility, the actual jet velocity will be lower. In addition, the shape of a jet modeled using the Bernoulli equation is that of a top hat with constant velocity within the jet and zero velocity outside. In reality, the jet will drag on the stationary air it encounters and will assume a parabolic velocity profile shortly after exiting the mouth as shown in Figure 7.4. Despite these shortcomings, most of the literature computes Strouhal number using the Bernoulli velocity. I re-plotted my reflection coefficient data against Strouhal number and found that the peaks all collapsed on one number, $St_W \approx .22$, which represents approximately half a wavelength fitting between the mouth and the labium. This demonstrates that there is a fairly specific physical situation for which the recorder will sound with little variation throughout its range. Figure 7.5 shows this transformation.

I was not satisfied, however, with assuming Bernoulli behavior for my jet, so I decided to install a Dwyer RMC-101 gas flow meter in line with my pressure source. I applied rising pressures to the head of the recorder attached to the AVNA and recorded the flow rate. As physically necessary, the velocity computed from the measured flow rate and cross section of the recorder head was below the Bernoulli velocity. Also as expected, the gap grew as the blowing pressure, and therefore the jet velocity, increased

typical alto by the time it reaches the labium. This effect would account for some acoustic differences and perhaps make the tenor sound "throatier". In addition, because $h = 0.8 * 10^{-3} meters$ and therefore $b = 0.4 * 10^{-3} meters$, $kb \approx 1$ for $St_W = 0.25$.

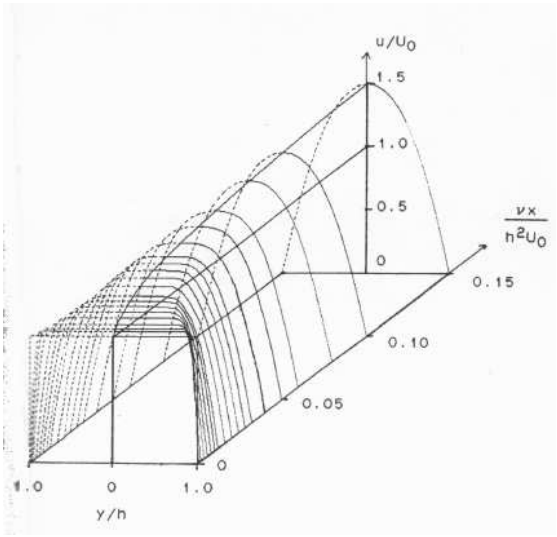

Figure 7.4: While the jet ideally leaves the mouth in a top hat velocity profile, as it exits viscous drag slows down the edges and the profile assumes a parabolic shape [18].

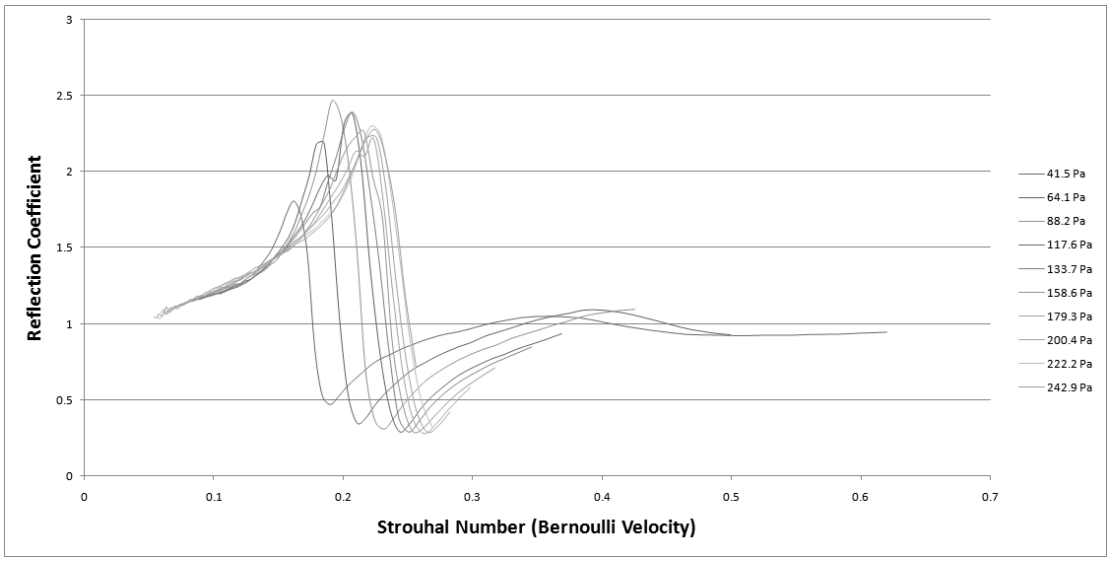

Figure 7.5: The Strouhal number is a dimensionless value that is approximately half as many wave lengths as fit between the mouth and the labium. Ideally, in a world without viscous and compressible air, the Strouhal number at the reflection coefficient maximum should be constant because it represents a specific number of wavelengths on the jet (See Figure 7.3 for slowly varying behavior). This plot demonstrates that while not constant, maximum reflection coefficients are reached at similar Strouhal numbers.

because the viscous drag increases with velocity. Figure 7.6 demonstrates these trends. Next, I redefined a new Strouhal number, which I call Measured Strouhal, $St_W Meas$, calculated with the measured mean velocity, and re-plotted my data. As shown in Figure 7.7, the peaks collapse even further, which means I had come even closer to finding the physical characterization of the conditions at which the recorder operates.

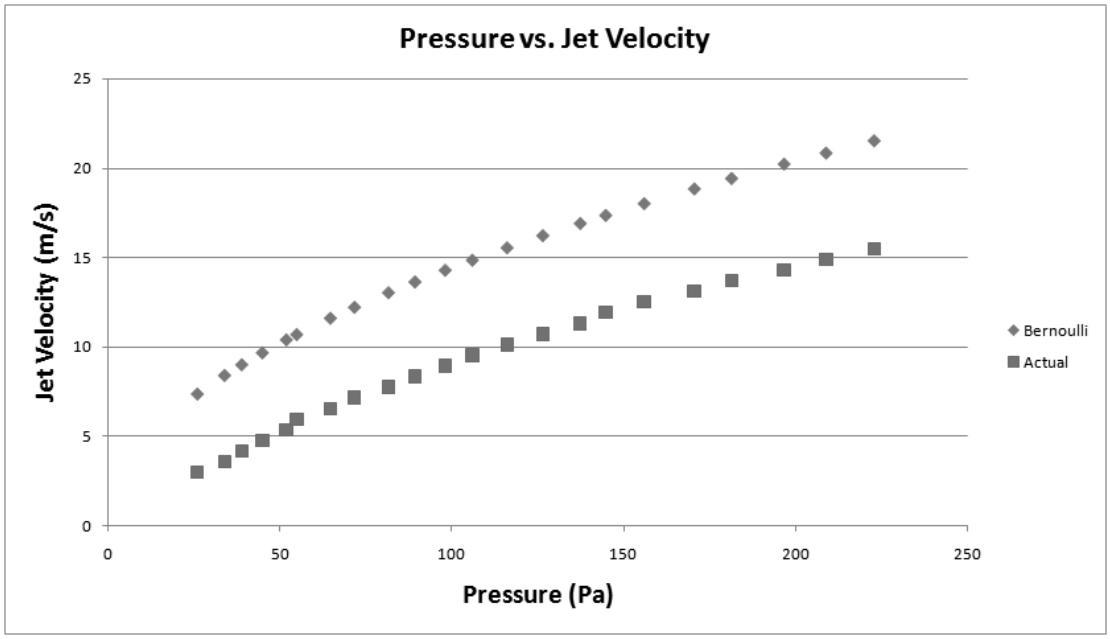

Figure 7.6: The Bernoulli velocity represents the maximum jet velocity; the measured velocity, the mean.

After calculating that the recorder should operate at a Strouhal number around 0.18 or a Measured Strouhal number around 0.25, I decided to examine the Schlieren images taken by M. P. Verge in his thesis to try and confirm my suspicions. He published the fundamental frequency of the disturbance, the blowing pressure, the absolute pressure of the first fundamental, and the Reynold's number

$$Re_h = \frac{U_j h}{\nu} \tag{7.4}$$

where U_j is the maximum jet velocity, h the jet height, and ν the kinematic viscosity, for each image. These data are enough for me to calculate the Strouhal

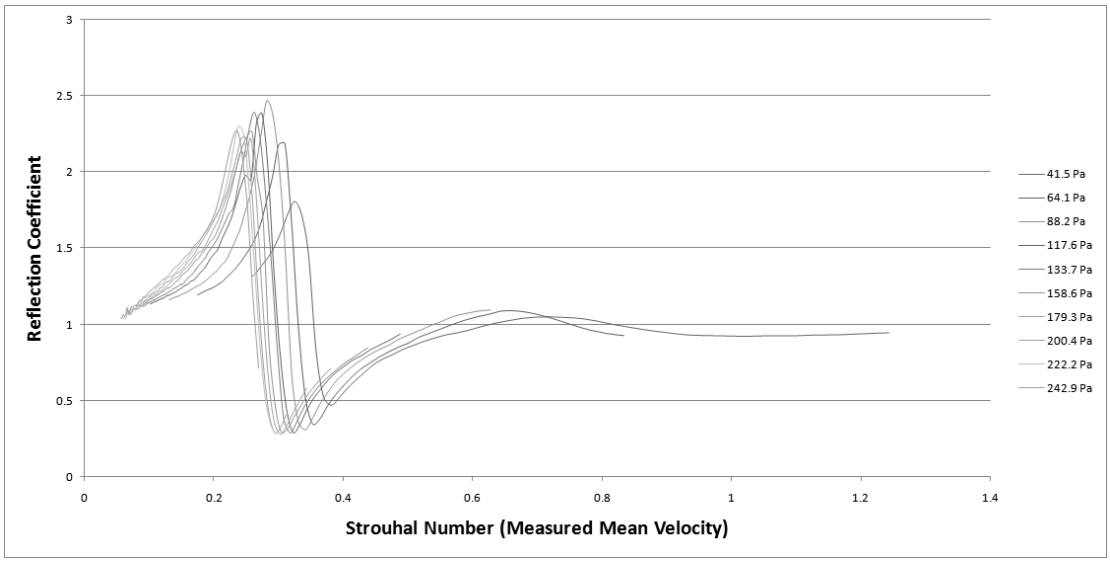

Figure 7.7: The peaks collapse even more when plotted against measured mean velocity. The Strouhal number is now less than half the number of wavelengths between the mouth and the labium because the average velocity is less than not only the Bernoully maximum velocity, but also the actual maximum on the jet.

Table 7.1: Verge's Schlieren images allow easy visualization of different Strouhal numbers.

Image	St_W	Blowing Pressure (Pa)	f_1 (Hz)	Acoustic Efficiency	$U_j \frac{m}{s}$
Figure 7.9	0.186	59	458	0.95	10.0
Figure 7.10	0.140	108	466	1.03	13.1
Figure 7.11	0.091	265	477	0.50	21.0
Figure 7.12	0.073	412	476	0.31	26.6
Figure 7.13	0.092	1058	960	0.40	42.3

number for each set of images and, using an acoustic efficiency defined as pressure out divided by blowing pressure, show where the instrument should operate. This fabricated acoustic efficiency

$$E_a = \frac{P_{f_1}}{P_b} \tag{7.5}$$

where P_{f_1} is the pressure of the first fundamental and P_b is the blowing pressure, is not a true power efficiency as usually defined in physics, but should give a rough sense of where the instrument operates most efficienty. Also, given the recorder has very weak harmonics relative to other instruments, Figure 7.8 compares the harmonics of the recorder to a trained opera singer, calculating efficiency using only the first fundamental seems reasonable. I found that Verge's acoustic efficiency is maximized at a Strouhal of 0.14 in Figure 7.10, which corresponds to $\frac{3}{8}$ of a wavelength on the jet. Because Verge used Bernoulli velocity, rather than measured mean, his Strouhal numbers should be increased by 50-100% to match my measurements, depending on blowing pressure. However, his images are what are important and he clearly shows a little less than half a wave on the jet at $St_W = 0.18$, which is approximately what I would have expected. Table 7.1 summarizes the data behind Verge's images.

After analyzing Verge's images, I turned to analyzing efficiency in my own data. I suspected that there would be a small range of Strouhal numbers for which the recorder would sound at all and an even small range for which the recorder would hit the right note. Furthermore, I noticed that once the Strouhal number strayed from that ideal

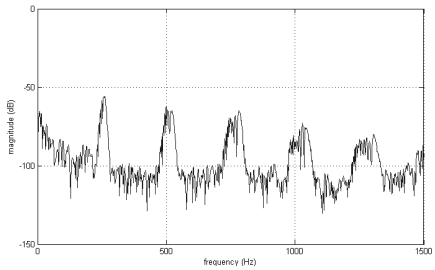

(a) 261 Hz Middle C Sung by Opera Singer

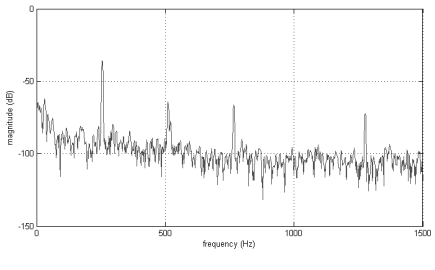

(b) 261 Hz Middle C Played with Tenor Recorder (uncorrected for temperature; actual frequency 255 Hz)

Figure 7.8: The opera singer's note contains far more and stronger harmonics than the recorder. Not only does this make the recorder a relatively easy instrument to study, but it validates my approach to calculating acoustic efficiency based on the first harmonic. Again, notes played using my pressure source sound lower, so had the air been at body temperature Subfigure 7.8(b) would have had its fundamental at 261 Hz rather than 255 Hz.

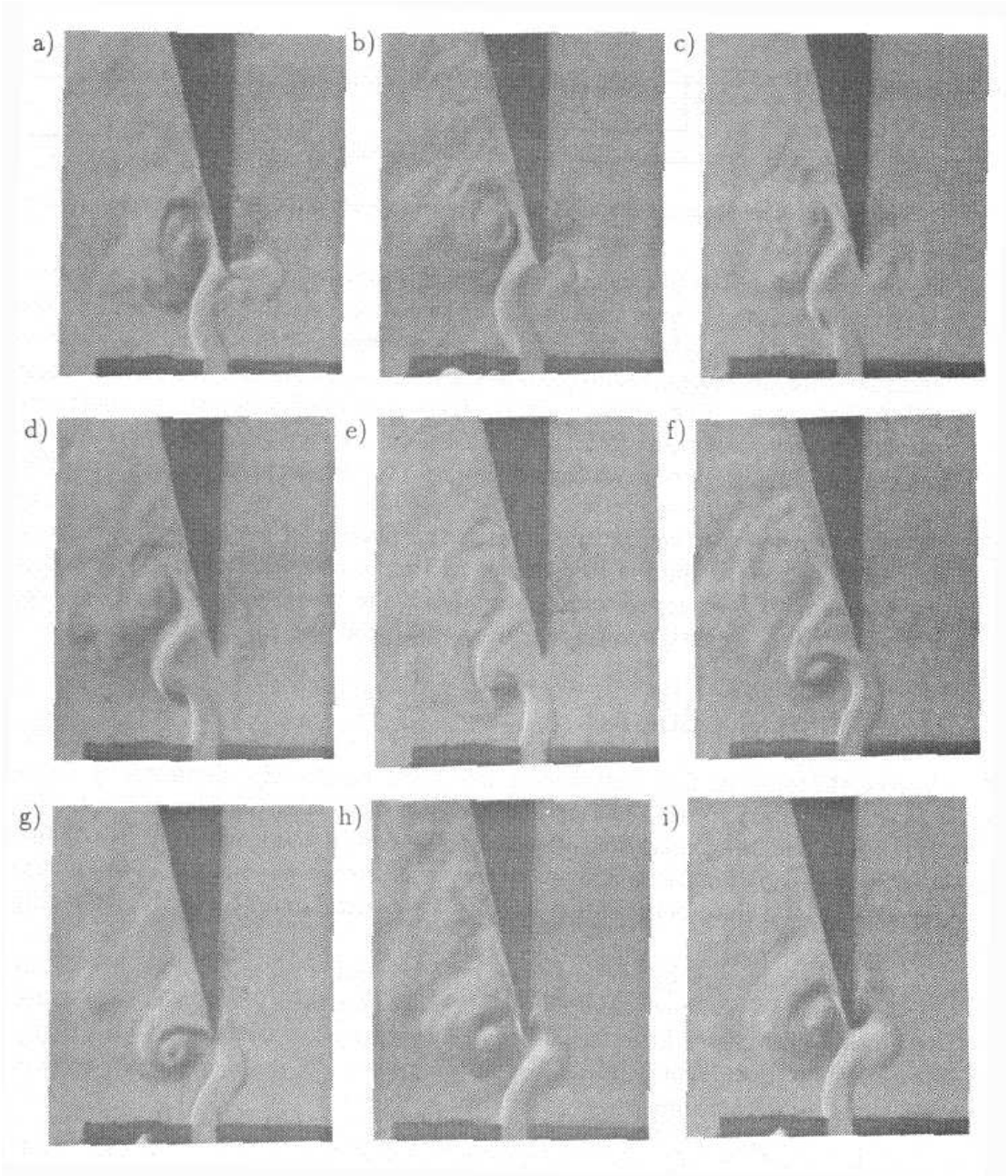

Figure 7.9: Schlieren images taken several hundred thousandths of a second apart for a blowing pressure of 59 Pa [9]. Close to half a wavelength fits between the mouth and the labium giving $St_W = 0.186$. The acoustic efficiency of this configuration is almost as good at $St_W = 0.140$ indicating that the window of acceptable Strouhal numbers extends up from 0.140.

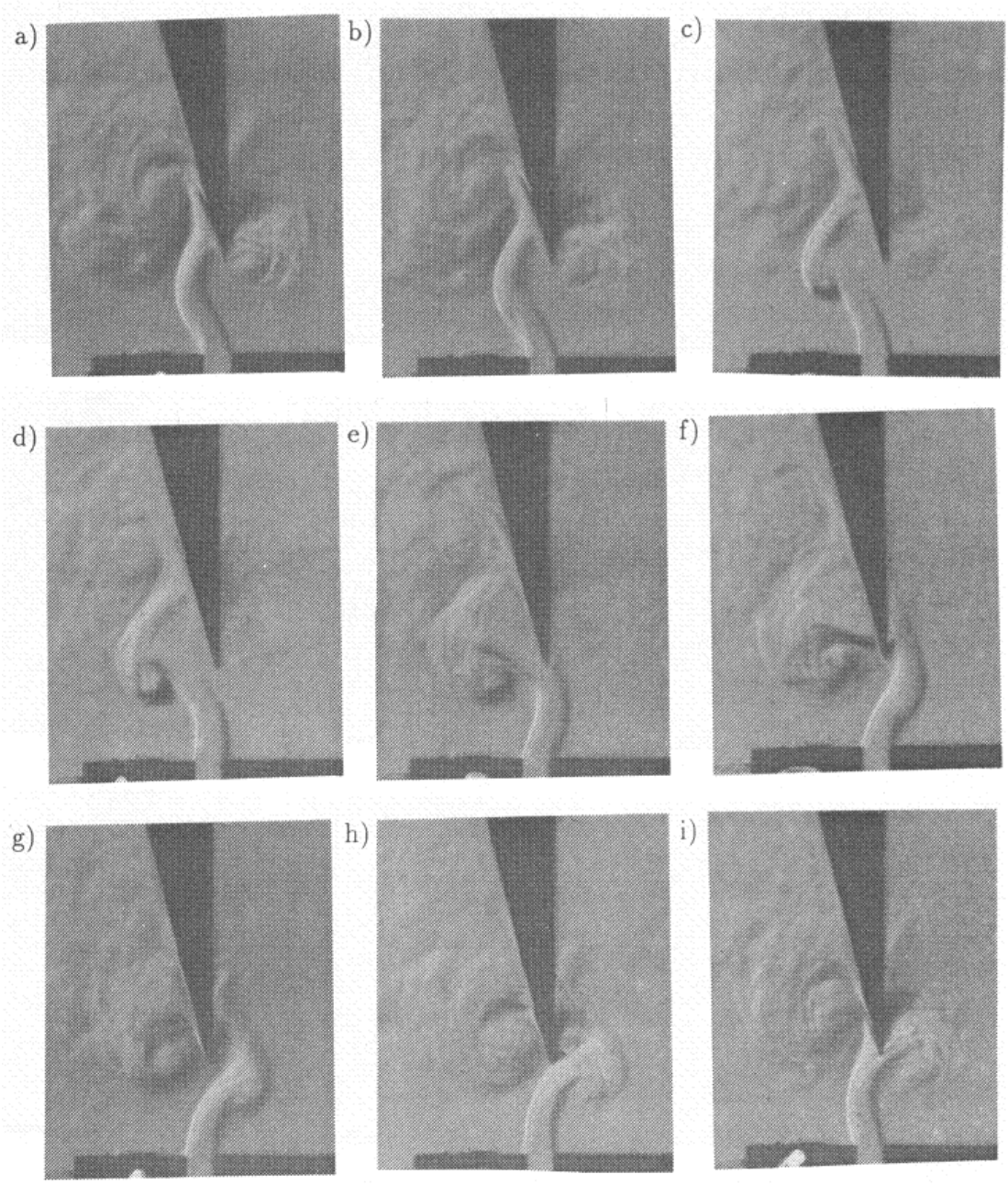

Figure 7.10: Schlieren images taken several hundred thousandths of a second apart for a blowing pressure of 108 Pa [9]. This blowing pressure demonstrated the highest acoustic efficiency.

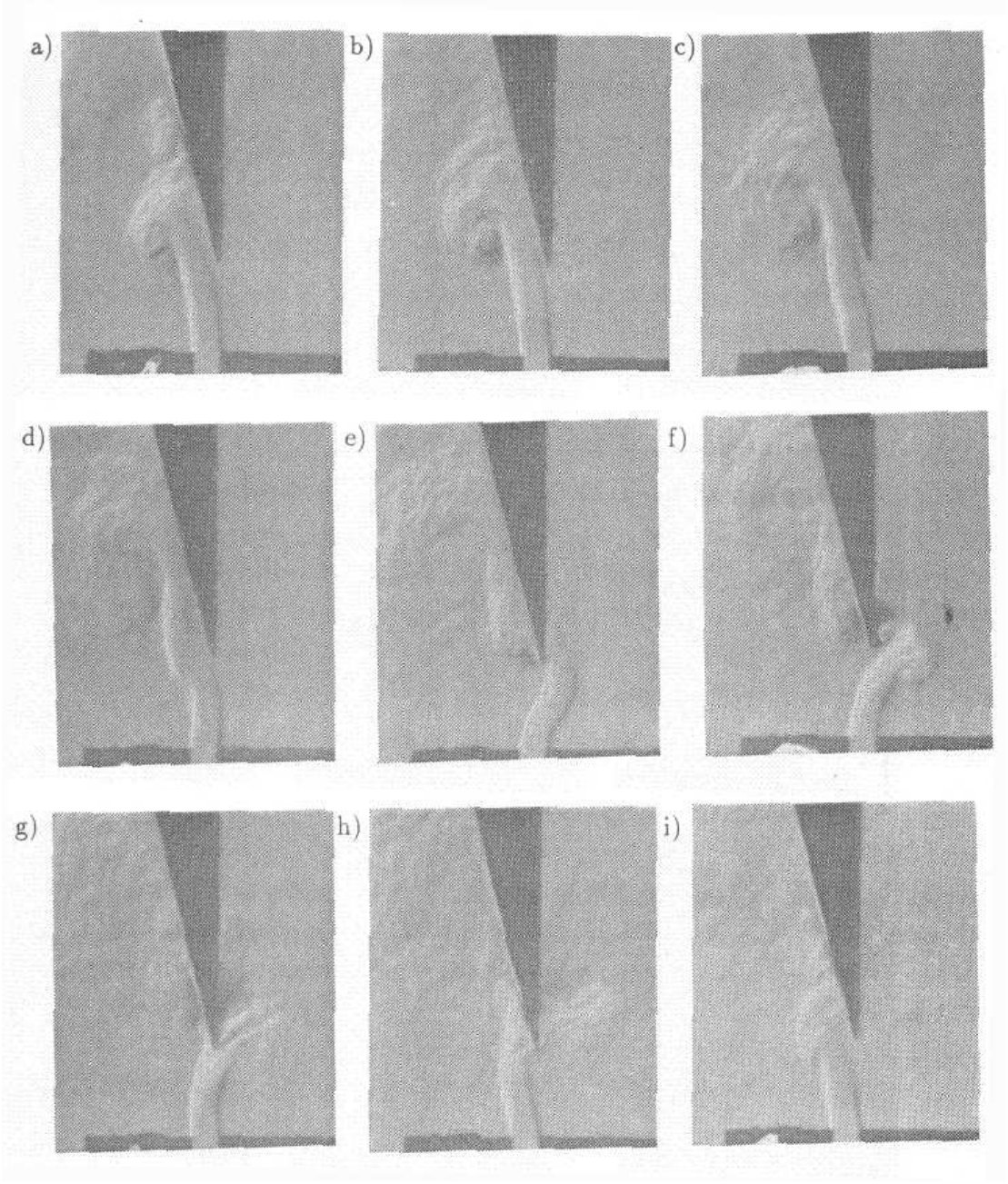

Figure 7.11: Schlieren images taken several hundred thousandths of a second apart for a blowing pressure of 265 Pa [9]. This is slightly above the highest blowing pressure I ever used. At this pressure the recorder is overblown in every fingering.

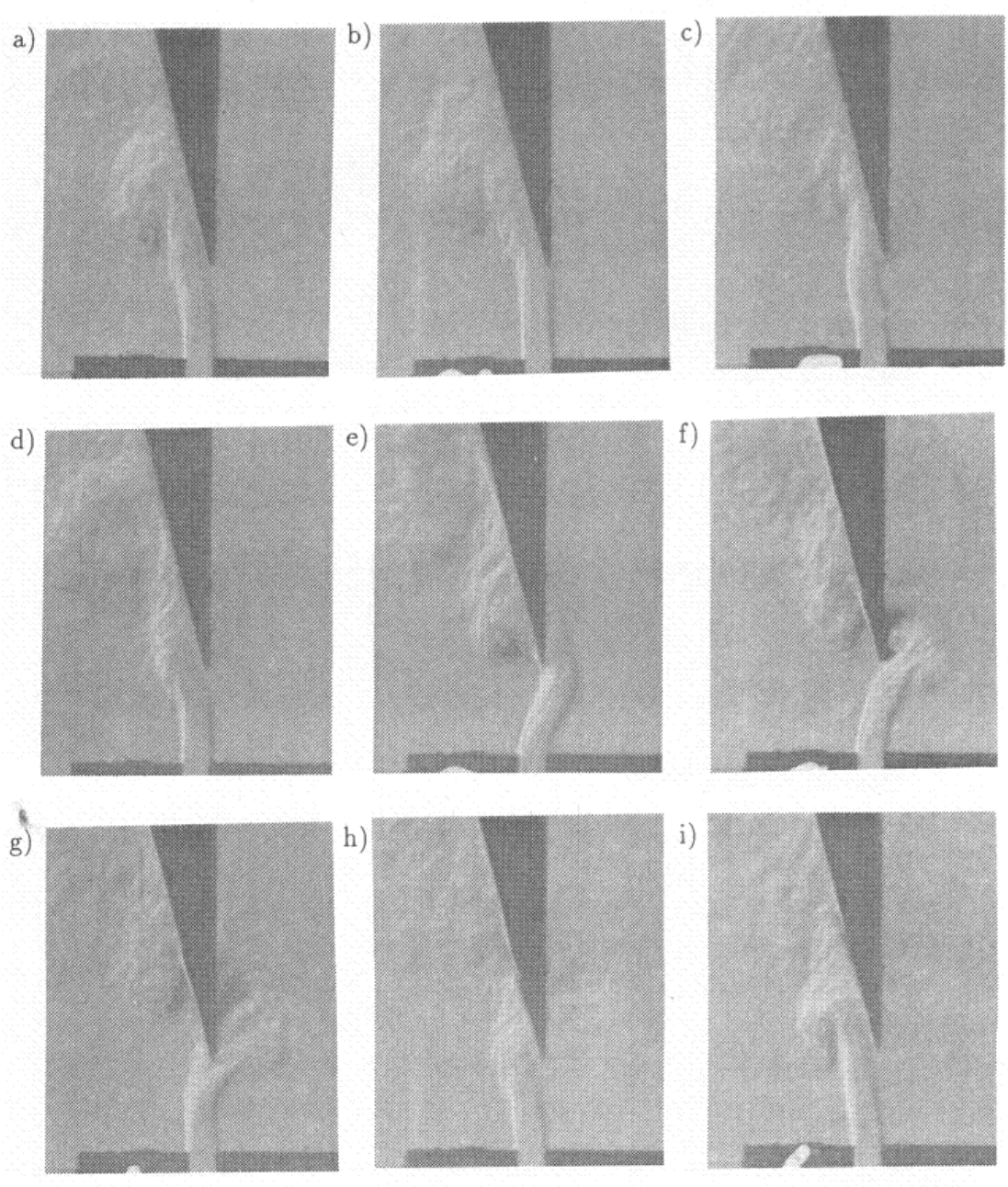

Figure 7.12: Schlieren images taken several hundred thousandths of a second apart for a blowing pressure of 412 Pa [9].

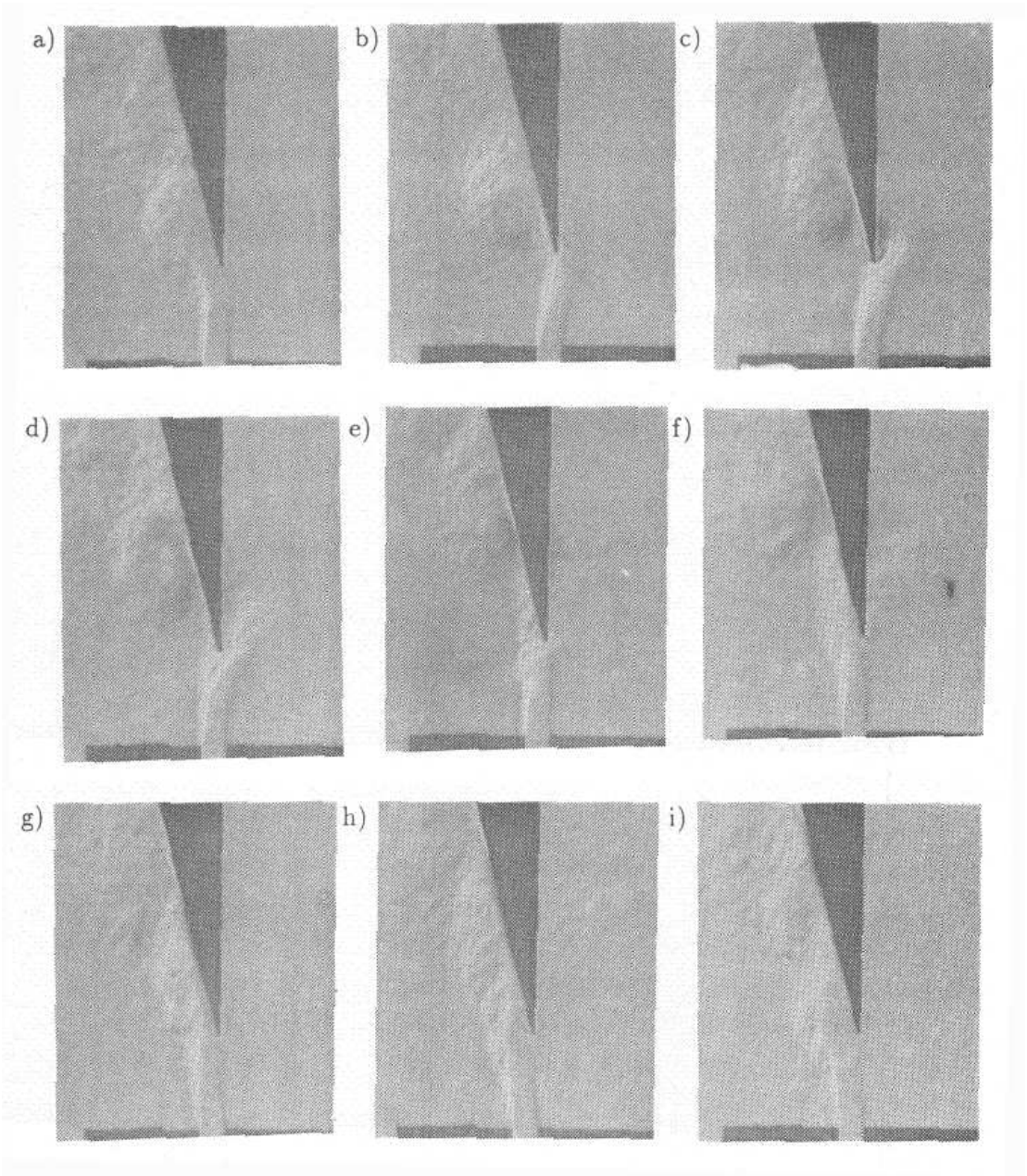

Figure 7.13: Schlieren images taken several hundred thousandths of a second apart for a blowing pressure of 1058 Pa [9]. At this point the resonator tube has jumped up to the next octave with $f_1 = 960Hz$.

value, my fabricated acoustic efficiency dropped. Verge did not provide enough data to calculate true power efficiencies, but given the relative calibration of my microphones and the fact that I can recorder both pressure and flow rate, I could run an efficiency experiment.

I taped all the holes of the fingered section of the recorder closed in the middle C configuration and measured power spectra from a barely audible blowing pressure to one hard enough to overblow to the next octave. I knew that acoustic power is pressure times flow rate, and that I could calculate relative power out by raising ten to the measured magnitude of the first fundamental divided by ten. In numbers

$$Power = P_b Q = k * 10^{\frac{f_1}{10}} \tag{7.6}$$

where P_b is pressure, Q is flow rate, k is a scaling constant necessary because the microphones are not absolutely calibrated, and f_1 the magnitude of the first fundamental. Therefore, my efficiency is shown in Equation 7.7

$$E = \frac{k * 10^{\frac{f_1}{10}}}{P_b Q} \tag{7.7}$$

I also knew that typical recorders have a power efficiency of about 1%, so I scaled k to reflect that value. Subfigure 7.8(b) shows the power spectrum of at a blowing pressure of 61.3 Pa. After calculating Measured Strouhal number, power in, and power out for each blowing pressure, I plotted Measured Strouhal number against efficiency and saw a peak at $St_W M = 0.18$, close to that computed using acoustic efficiency and Verge's images as shown in Figure 7.14.

Remarkably, once corrected for air temperature, the blowing pressure that exhibited the greatest efficiency also sounded exactly 261 Hz, the accepted frequency of the middle C. I did not have time to extend this experiment to other fingerings, but it suggests that efficiency and frequency are closely linked.

A final element of my investigation was into the effect, if any, of forked fingerings on the effective length of the recorder. Recorders are fairly unique in that some notes

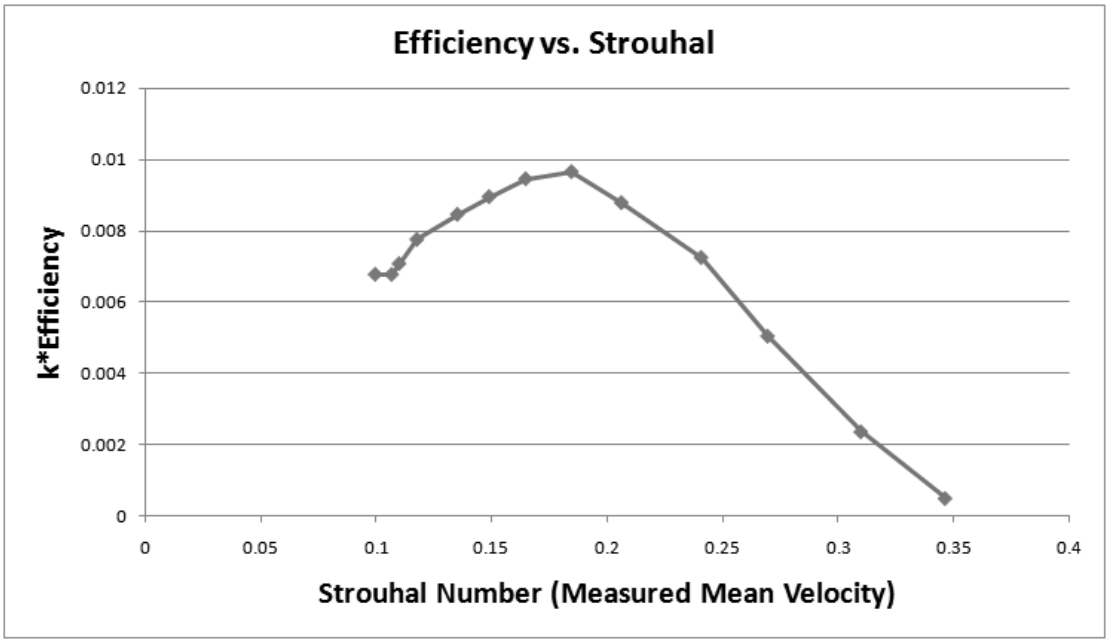

Figure 7.14: Power efficiency peaks at a $St_W M \approx 0.18$. Serendipitously, at that Measured Strouhal number, the note is perfectly in tune.

require a hole to be left open in between two closed holes as show in Figure 7.15. Using the AVNA and tape to close different holes, I measured the reflection coefficient of the tenor recorder's entire bottom octave from C4 to C5. I then set the reference plane to best approximate a closed end and recorded the values. Despite the forked fingerings and other oddities of recorder design, there was a very linear reduction in resonator tube length as I moved up the scale (see Figure 7.16).

Figure 7.15: Certain notes require "forked fingerings" in which a hole is left open between two closed holes.

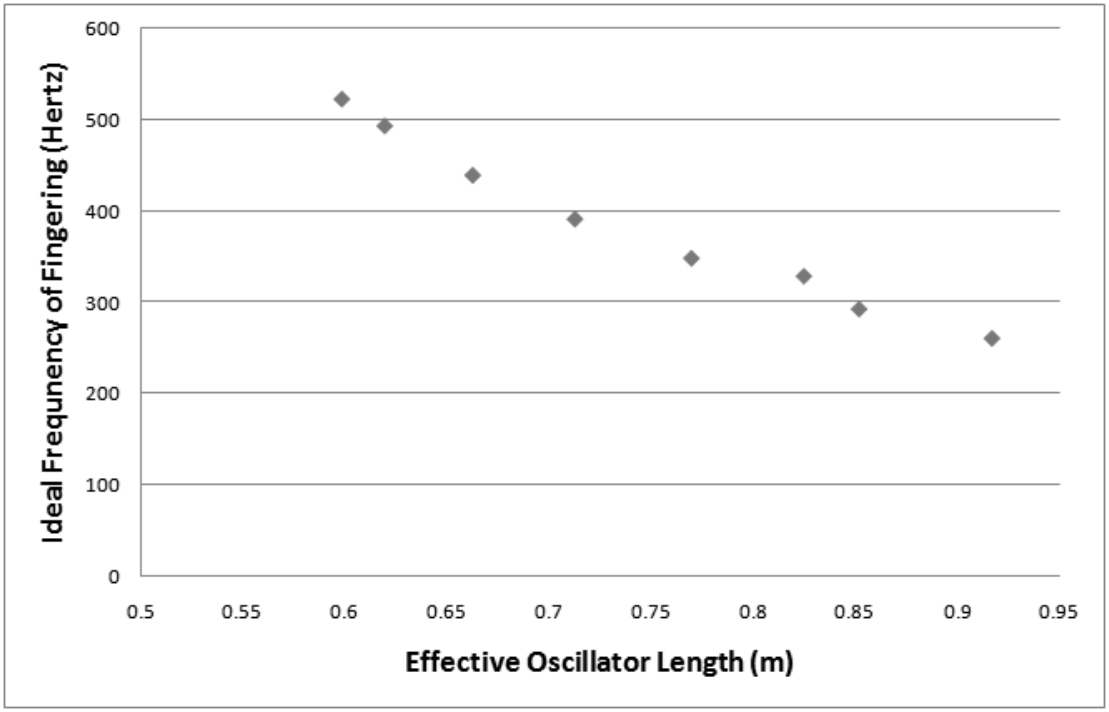

Figure 7.16: As the ideal frequency of a given fingering increases, the length of the tube decreases, despite strange forked fingerings.

Chapter 8

Conclusion

After looking at the reflection of an air-jet from a frequency, Strouhal number, visual, and efficiency perspective, it is safe to say that recorder behavior is closely tied to the number of wavelengths on the jet that fit between the mouth and the labium. While the reflection data show a maximum gain at Strouhal number around 0.2, depending on whether mean or theoretical maximum jet velocity is used, the Schlieren images taken by Verge and my own data show a maximum efficiency at around 0.15. This puzzles me as I would have expected the same situation that would maximize gain would also maximize efficiency, but there is no physical law requiring it. Perhaps involved is the fact that radiation efficiency increases rapidly with frequency. The data showing that a perfectly sounded note occurs at a point of maximum efficiency suggest that efficiency should be investigated further. The fact remains, however, that I have shown that under normal operation, the Strouhal number stays somewhere between 0.12 and 0.25. It is known that the recorder is a complicated instrument and it is quite possible that different notes require a range of Strouhal numbers leading to varying efficiencies and blowing pressures. While I have answered quite a few questions related to flue instruments, I have raised even more. In the future I would like to investigate why reflection coefficient peaks at 500 Hz, well below the typical playing range, how the width of the reflection coefficient affects the sound, and the roles of turbulence in sound production. It is quite possible that all these effects stem from the recorder's long evolution, rather than a

series of logical decisions, and exist simply because the instrument works the way it is. Further research is certainly needed before our Yamaha engineer can finish his project.

Bibliography

[1] Lindsay, R. B. Journal of the Acoustic Society of America **36**, 2242 (1964).

[2] Maris, H. J. Journal of Low Temperature Physics **93**, 355–364 (1993).

[3] Fabre, B. and A., H. Journal of the Acoustic Society of America **6.8**, 983–992 (2000).

[4] Lindsay, R. B. Historical Introduction to the Theory of Sound. Dover Publications, New York, (1945).

[5] Rossing, T. D. Springer Handbook of Acoustics. Springer, New York, (2007).

[6] Gafurio, F. Theorica Musice.

[7] Coltman, J. Journal of the Acoustic Society of America **6.8**, 983–992 (1968).

[8] de la Cuadra, P. The Sound of Oscillating Instruments: Physics, Modeling, and Simulation in Flute-Like Instruments. PhD thesis, Stanford University, (2006).

[9] Verge, M.-P. Aeroacoustics of Confined Jets with Applications to the Physical Modeling of Recorder-Like Instruments. PhD thesis, Techische Universiteit Eindhoven, (1995).

[10] Fletcher, N. Journal of the Acoustic Society of America **74(2)**, 400–408 (1983).

[11] Benade, A. Journal of the Acoustic Society of America **44(2)**, 616–623 (1968).

[12] Wittmann, M. Acoustic Vector Network Analysis. PhD thesis, University of Colorado, (2009).

[13] Price, J. Acoustic VNA User's Guide. University of Colorado, Boulder, (2008).

[14] Strutt, John William, B. R. The Theory of Sound. Dover Publications, New York, (1945).

[15] Coltman, J. Journal of the Acoustic Society of America **69**, 1164–1168 (1981).

[16] Fletcher, N. The Physics of Musical Instruments. Springer-Verlag, New York, (1991).

[17] Bernoulli, D. Hydrodynamica. Readex Microprint, New York, (1973).

[18] Martin, J. The Acoustics of the Recorder. Moeck Verlag, Germany, (1994).